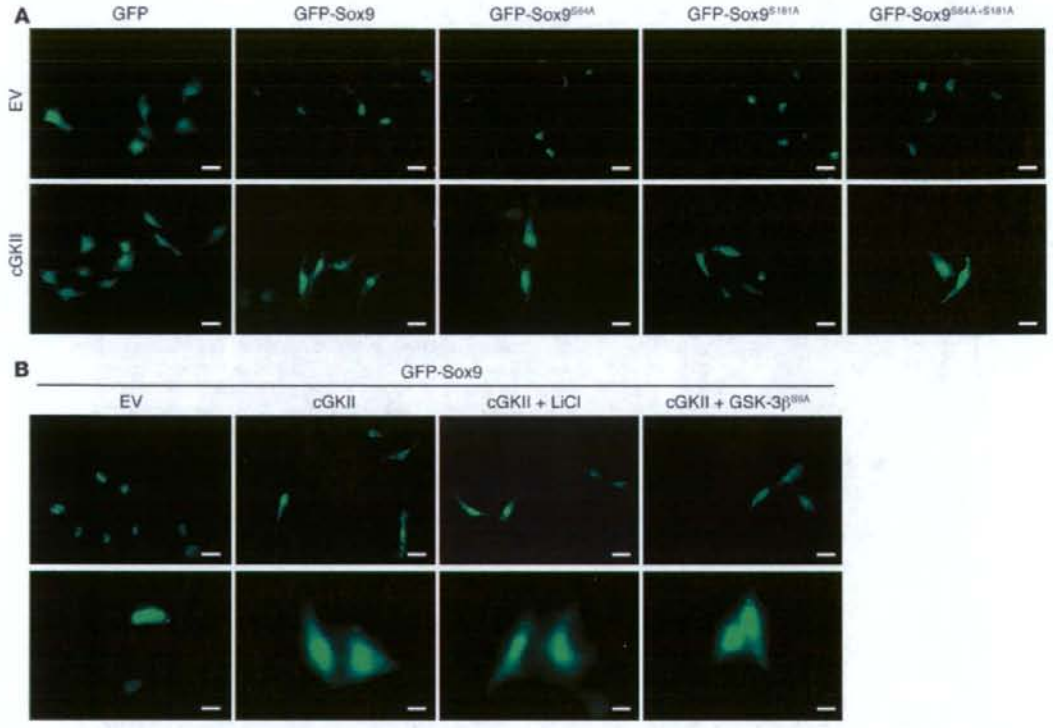


**Figure 5**

Subcellular localization of Sox9. (**A**) Effect of cGKII on subcellular localization of Sox9 and the phosphorylation-deficient mutants at putative phosphorylation sites at Ser64 ($Sox9^{S64A}$), Ser181 ($Sox9^{S181A}$), or both ($Sox9^{S64A+S181A}$). HeLa cells were transfected with GFP, GFP-tagged Sox9 (GFP-Sox9), or the GFP-tagged mutants in combination with cGKII or empty vector. Subcellular localization of Sox9 or the mutants was determined by a fluorescent microscope. (**B**) Effect of LiCl treatment or $GSK\text{-}3\beta^{S9A}$ transfection on Sox9 subcellular localization in HeLa cells cotransfected with GFP-tagged Sox9 in combination with cGKII or empty vector. Scale bars: 10 μm (**A**); 20 μm (**B**, top); 5 μm (**B**, bottom).

membranous ossification (11, 18) — were comparable to those of WT littermates (Figure 6C). The genetic insufficiency of GSK-3β in the *Prkg2*$^{-/-}$ *Gsk3b*$^{+/-}$ mice partially, but significantly, restored the impaired skeletal growth (about 20%–40%). These findings indicate that sufficient GSK-3β function is needed for skeletal growth and endochondral ossification to be impaired by cGKII deficiency.

Further histological analyses revealed that the elongated growth plate and decreased COL10 expression in *Prkg2*$^{-/-}$ mice were also partially restored in the *Prkg2*$^{-/-}$ *Gsk3b*$^{+/-}$ mice (Figure 7, A and B). In contrast, GSK-3β insufficiency did not alter skeletal growth or growth plate parameters in WT or *Prkg2*$^{+/-}$ mice, as shown in *Gsk3b*$^{+/-}$ and compound *Prkg2*$^{+/-}$ *Gsk3b*$^{+/-}$ mice, respectively (Supplemental Figure 3). GSK-3β may therefore function specifically as a mediator of cGKII signaling, rather than generally in the regulation of chondrocyte hypertrophy and endochondral ossification.

## Discussion

Based on our previous finding that cGKII activity is essential for the promotion of skeletal growth through hypertrophic differentiation of growth plate chondrocytes (9), the results of our present study initially identified GSK-3β as a likely substrate of this protein kinase. Figure 7C summarizes the mechanism underlying chondrocyte hypertrophy by cGKII/GSK-3β signaling based on the present and previous studies. cGKII phosphorylates GSK-3β at Ser9 and inactivates it, which may contribute to the suppression of β-catenin degradation, as previously reported (10). We and others have reported that β-catenin/TCF signaling causes stimulation of hypertrophic differentiation of chondrocytes in vitro (19–22). In addition, chondrocyte-specific inactivation of β-catenin in mice results in dwarfism with delayed hypertrophic differentiation of chondrocytes (23). Hence, the stabilization and accumulation of β-catenin by cGKII/GSK-3β signaling in chondrocytes may lead to hypertrophic differentiation, although the underlying molecular mechanism is still controversial.

Genetic rescue of impaired skeletal growth in *Prkg2*$^{-/-}$ mice by suppression of GSK-3β was significant, but incomplete (Figures 6 and 7). This might be because GSK-3β haploinsufficiency was inadequate to fully overcome the deficiency of cGKII. Indeed, cultured *Gsk3b*$^{+/-}$ chondrocytes showed higher COL10 expression, but similar ALP and MMP-13 expression, compared with WT cells, while LiCl clearly increased all hypertrophic markers in the ATDC5 cell culture (Figure 3, A and C). We cannot exclude the possibil-

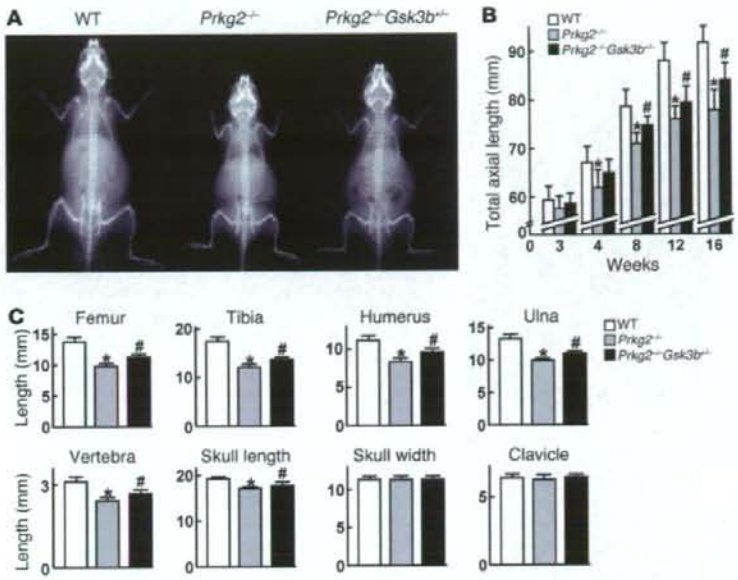


**Figure 6**
Genetic rescue of growth retardation in *Prkg2*$^{-/-}$ mice by GSK-3β insufficiency. (**A**) Radiographs of WT, *Prkg2*$^{-/-}$, and *Prkg2*$^{-/-}$ *Gsk3b*$^{+/-}$ littermates at 8 weeks of age. (**B**) Time course of total axial length (from nose to tail end) of the 3 genotypes from 3 to 16 weeks of age. The recovery by the GSK-3β insufficiency in the *Prkg2*$^{-/-}$ mice was 43.2%, 31.4%, and 41.9% at 8, 12, and 16 weeks, respectively. (**C**) Length of bones of the 3 genotypes at 8 weeks of age. Percent recovery was 21.7%, 18.3%, 24.3%, 16.2%, 24.3%, and 42.6% in femur, tibia, humerus, ulna, vertebra, and skull length, respectively. Data are mean ± SD for 4–9 mice per genotype. *$P < 0.05$ versus WT. #$P < 0.05$ versus *Prkg2*$^{-/-}$.

ity, however, of involvement of other mechanisms in the actions of cGKII on chondrocyte hypertrophy. Although our previous study showed that cGKII phosphorylated Sox9, an inhibitor of chondrocyte hypertrophy, and suppressed its nuclear entry (9), the present study revealed that the subcellular translocation was not mediated by the phosphorylation of Sox9 itself or of GSK-3β (Figure 5). Besides Sox9 and GSK-3β, VASP and cysteine- and glycine-rich protein 2 have previously been reported as phosphorylation targets of cGKII in other types of cells (24). However, our luciferase assays failed to show regulation of COL10 transcription by either gene (Figure 2B and Supplemental Figure 2B), suggesting the existence of other phosphorylation targets of cGKII in the regulation of Sox9 translocation associated with chondrocyte hypertrophy. In addition, because Sox9 has previously been reported to physically interact with β-catenin and to compete with its binding to TCF (23), the downstream pathways of cGKII through GSK-3β and Sox9 might interact at the level of β-catenin during chondrocyte hypertrophy.

Chondrocyte hypertrophy in the growth plate is a rate-limiting step for longitudinal skeletal growth (25), because this step has been shown to be responsible for 40%–60% of endochondral ossification, with the remainder caused by chondrocyte proliferation and matrix synthesis (26). Sox9 is a representative regulator of this step, as are Runx2 (1, 13) and parathyroid hormone/parathyroid hormone–related protein (PTH/PTHrP) (1, 27), uncovered via recent advances in molecular genetics. The present study failed to find interaction between cGKII and Runx2 (Supplemental Figure 1). Although PTH/PTHrP has previously been shown to be a potent inhibitor of chondrocyte hypertrophy by the findings in deficient and transgenic mice (1, 27), our previous study revealed that neither expression levels of PTHrP and PTH/PTHrP receptor nor cAMP accumulation by PTH stimulation was altered by cGKII deficiency in chondrocytes (9). Hence, cGKII may regulate chondrocyte hypertrophy by a mechanism independent of those of Runx2 and PTH/PTHrP.

In line with the view that cGKII is a downstream mediator of CNP, *Nppc*$^{-/-}$ and *Npr2*$^{-/-}$ mice also exhibit dwarfism (2). However, unlike *Prkg2*$^{-/-}$ mice, which have an elongated growth plate with an abnormal intermediate layer, both *Nppc*$^{-/-}$ mice and *Npr2*$^{-/-}$ mice showed thinned growth plates with chondrocytes arranged in a regular columnar array. This may indicate the involvement of other signaling pathways in CNP/GC-B–mediated endochondral ossification. In fact, the intracellular accumulation of cGMP caused by CNP/GC-B signaling activates not only cGKII, but also other downstream mediators, such as cGKI, cyclic nucleotide phosphodiesterases, and cGMP-regulated ion channels (5, 28). Although no skeletal abnormality has been reported in *Prkg1*$^{-/-}$ mice (8), it would be helpful to investigate whether mice doubly deficient for cGKI and cGKII mimic the phenotype of *Nppc*$^{-/-}$ or *Npr2*$^{-/-}$ mice. In addition, targeted overexpression of CNP in growth plate chondrocytes was reported to restore the achondroplastic bone with FGF receptor 3 mutation through inhibition of the MAPK pathway (15), which we found in the present study to be unrelated to cGKII (Supplemental Figure 2A). Furthermore, cGKII functions as an effector of cGMP that is activated not only by CNP, but also by nitric oxide and other types of natriuretic peptides (5, 7, 28). Although the fact that CNP was unable to affect chondrocyte differentiation of skeletal growth in the absence of cGKII either in vitro or in vivo indicates a crucial role of cGKII in CNP signaling (29), CNP and cGKII are unlikely to function with a one-to-one correspondence during endochondral ossification.

The abnormal elongation of the *Prkg2*$^{-/-}$ mouse growth plate was apparent from 2 to 4 weeks after birth, but not before or after these ages (Figure 1B). This observation suggests some compensatory mechanisms for cGKII deficiency. Besides signaling via Runx2, PTH/PTHrP, and the CNP-related factors described above, GSK-3α (the other GSK-3 in mammals) might substitute for GSK-3β, because it was not found to be a phosphorylation target of cGKII (Figure 2D). Although there was no compensatory upregulation in

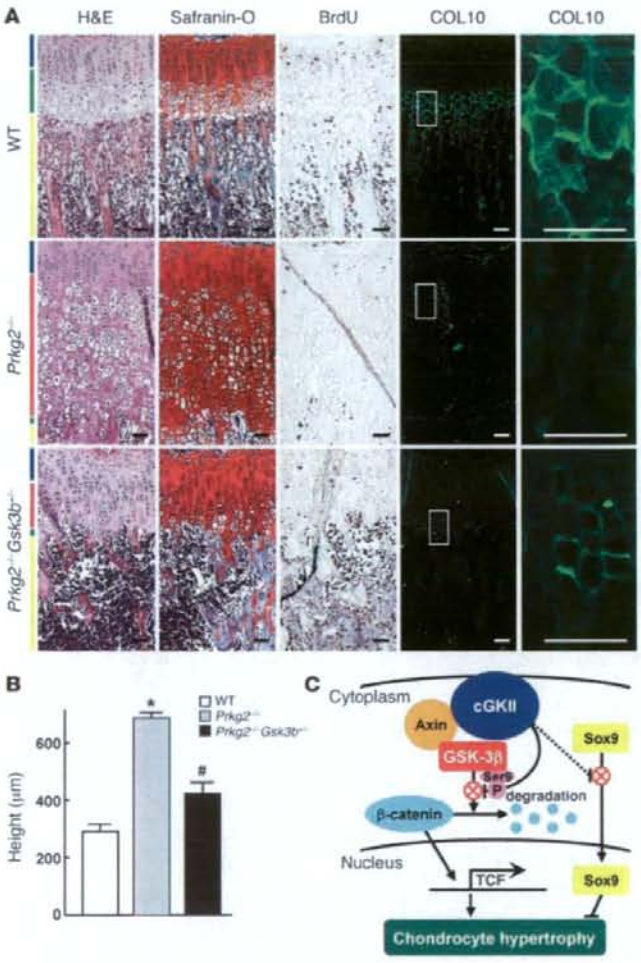


**Figure 7**
Genetic rescue of growth plate abnormality in *Prkg2*$^{-/-}$ mice by GSK-3β insufficiency. (**A**) H&E staining, Safranin-O staining, BrdU labeling, and immunohistochemical staining of COL10 in the tibial growth plates of 3-week-old mice of the 3 genotypes. Blue, red, green, and yellow bars indicate proliferative zone, abnormal intermediate layer, hypertrophic zone, and primary spongiosa, respectively. Boxed regions in COL10 panels are shown at higher magnification to the right. Scale bars: 50 μm. (**B**) Height of the growth plates of the 3 genotypes. The percentage recovery by the GSK-3β insufficiency was 36.0%. Data are mean ± SD of 4 mice per genotype. *$P < 0.05$ versus WT. #$P < 0.05$ versus *Prkg2*$^{-/-}$. (**C**) Schematic of the mechanism whereby cGKII promotes growth plate chondrocyte hypertrophy during skeletal growth.

GSK-3 levels in cells lacking either GSK-3α or GSK-3β, functional redundancy of the 2 GSK-3 homologs in β-catenin/TCF–mediated transcription was previously shown using an allelic series of embryonic stem cell lines (17, 30). In fact, *Gsk3b*$^{+/-}$ mice (Supplemental Figure 3) and *Gsk3a*$^{+/-}$ mice (31) showed normal skeletal development and growth. *Gsk3b*$^{+/-}$ mice developed relatively normally until late gestation, when massive liver apoptosis causes embryonic lethality (17); the implication of this finding is that GSK-3α can compensate for GSK-3β deficiency in early stages of mouse development, but cannot substitute for it in all respects. Hence, the age-dependent balance between GSK-3α and GSK-3β might explain the temporary growth plate abnormality in *Prkg2*$^{-/-}$ mice.

GSK-3β is known to be active under resting conditions and inactivated upon stimulation by several signaling pathways, such as Wnt and insulin/Akt; however, the role of phosphorylation of GSK-3β remains controversial (32, 33). Our present results led us to propose cGKII as a novel regulator of GSK-3β and showed that the β-catenin activity enhanced by cGKII was suppressed by GSK-3β$^{S9A}$, indicating the mediation of GSK-3β phosphorylation at Ser9 in cGKII/β-catenin signaling (Figure 4C). Conversely, several reports showed that GSK-3β inactivation causing β-catenin induction by Wnt stimulation depends not on Ser9 phosphorylation, but rather on coupling with the scaffolding protein, such as Axin (34, 35). The present study, however, showed that cGKII formed a complex with Axin and further phosphorylated GSK-3β that bound to Axin (Figure 4D), suggesting some interaction between Ser9 phosphorylation and coupling with Axin in the regulation of GSK-3β by cGKII. In fact, a previous report proposed that Wnt signaling, similar to insulin/Akt signaling, induces GSK-3β phosphorylation via the interaction between the signaling pathways both in neuronal PC12 cells and in human embryonic kidney 293T cells (36). While these findings imply a possible link between cGKII/β-catenin and canonical Wnt/β-catenin signaling, we note that there is no direct evidence of cGKII being involved in the canonical Wnt pathway. We therefore believe that cGKII/β-catenin signaling, which is dependent on GSK-3β phosphorylation, may have a mechanism that is, at least in part, distinct from that of Wnt/β-catenin signaling. Further studies will be needed to clarify the details of GSK-3β–related signaling not only in chondrocytes, but also in other cells.

We conclude that cGKII promotes chondrocyte hypertrophy and skeletal growth through phosphorylation and inactivation of GSK-3β. For the application of this intracellular signaling to yield novel therapeutics for skeletal disorders, we are now developing a gene transfer system using biocompatible polyplex nanomicelles (37, 38). Further understanding of the molecular signaling related to the cGKII/GSK-3β axis, in combination with other putative signaling systems, will greatly assist in unraveling the molecular network that modulates endochondral ossification and skeletal growth.

## Methods

*Animals.* The *Prkg2*$^{+/-}$ mice and *Gsk3b*$^{+/-}$ mice were maintained in a C57BL/6 background. To generate *Prkg2*$^{-/-}$*Gsk3b*$^{+/-}$ mice, *Gsk3b*$^{+/-}$ mice were mated with the homozygous *Prkg2*$^{-/-}$ mice to obtain *Prkg2*$^{+/-}$*Gsk3b*$^{+/-}$ mice, which were then mated with each other. All experiments were performed on male mice and were approved by the Animal Care and Use Committee of the University of Tokyo.

*Radiological and histological analyses.* Plain radiographs were taken using a soft X-ray apparatus (Softex CMB-2; Softex). For histological analyses, skeletons were fixed in 4% paraformaldehyde, decalcified with 10% EDTA, embedded in paraffin, sectioned in 5-μm slices, and stained with H&E or Safranin-O, according to standard procedures. For BrdU labeling, mice were injected intraperitoneally with BrdU (25 μg/g body weight) 2 h prior to sacrifice, and the sections were stained with a BrdU staining kit (Zymed Laboratories) according to the manufacturer's instructions. In situ hybridization with nonradioactive probes was performed as previously described (39). For immunohistochemistry, antibodies to cGKII, Ser9-phosphorylated GSK-3β, MMP-13, Runx2 (1:50; Santa Cruz Biotechnology Inc.), GSK-3β (1:200; Chemicon), COL10 (1:1000; LSL), β-catenin (1:100; Cell Signaling Technology), and respective nonimmune serums were used, and the signal was detected with an HRP-conjugated secondary antibody. For fluorescent visualization, a secondary antibody conjugated with Alexa Fluor 488 (Invitrogen) was used.

*Cell cultures.* ATDC5 cells were grown and maintained in DMEM and F12 at a 1:1 ratio with 5% FBS. To induce hypertrophic differentiation, the ATDC5 cells were cultured in the presence of insulin, transferrin and sodium selenite (ITS) supplement (Sigma-Aldrich) for 21 d as described previously (40). We confirmed COL10 expression by real-time RT-PCR and used the cells whose stage of differentiation was assumed to be prehypertrophic or hypertrophic. Primary chondrocytes were isolated by digestion of E18.5 costal cartilage. Primary chondrocytes, HuH-7 cells, HEK293 cells, and HeLa cells were cultured in high-glucose DMEM with 10% FBS. Three-dimensional alginate bead cultures of primary costal chondrocytes and ATDC5 cells were performed with or without LiCl (8 mM) for 72 h, and the cells were analyzed as described previously (21). For immunocytochemistry of primary costal chondrocytes, the cell colonies were fixed with 4% paraformaldehyde, embedded in paraffin, sectioned in 5-μm slices, and underwent immunostaining for COL10 and MMP-13 as described above. For ALP staining, sections were fixed in 70% ethanol and stained for 10 min with a solution containing 0.01% Naphthol AS-MX phosphate disodium salt (Sigma-Aldrich), 1% N, N-dimethyl-formamide (Wako Pure Chemical Industries Ltd.), and 0.06% fast blue BB (Sigma-Aldrich).

*In vitro kinase assay.* ATDC5 cells were cultured in the presence of ITS for 21 d to differentiate into prehypertrophic or hypertrophic chondrocytes, as described above. The whole-cell lysate of the differentiated cells was prepared using Cell Lysis Buffer (Cell Signaling Technology). The cell lysate or recombinant GSK-3β (Upstate Biotechnology Inc.) was incubated with recombinant cGKII (Sigma-Aldrich) in a reaction buffer (Cell Signaling Technology) containing 1.6 mM ATP and 100 μM 8-bromo-cGMP (Biomol) at 30°C for 30 min. An equal amount of protein (15 μg) was subjected to SDS-PAGE and transferred onto nitrocellulose membranes. IB was then performed using primary antibodies to Ser9-phosphorylated GSK-3β (Cell Signaling Technology), GSK-3β (Chemicon), Ser21-phosphorylated GSK-3α and GSK-3α (Cell Signaling Technology), and β-actin (Sigma-Aldrich). The membrane was incubated with HRP-conjugated antibody (Promega), and the immunoreactive proteins were visualized with ECL Plus (Amersham Biosciences).

*Plasmids and viral vectors.* cDNA of caspase-9 (GenBank accession no. NM_001229.1), Bad (NM_007522.2), PLK (NM_011121.3), p90RSK (NM_009097.4), eNOS (NM_000603.3), GSK-3β (NM_002093.2), VASP (NM_009499.1), cdc25 (NM_009860.2), and cysteine- and glycine-rich protein 2 (CSRP2; NM_007792.3) was ligated into pCMV-HA (Invitrogen). cDNA of rat cGKII (NM_013012.1; nucleotides 48–2,333) was ligated into pcDNA4HisA (Invitrogen). A PCR-amplified fragment (nucleotides 48–1,403) was used to construct the cGKII-Δkinase plasmid. Plasmids encoding constitutively active human cGKII were kindly provided by B.M. Hogema (Erasmus University Medical Center, Rotterdam, The Netherlands; ref. 41). Axin1 (NM_003502.2) was subcloned into pCMV-Myc (Invitrogen) to introduce Myc epitope tags. cDNA of Sox9 (NM_000346.2) and Runx2 (NM_009820.3) was ligated into pEGFPC1 (Clontech) to generate GFP-tagged plasmids. To create phosphorylation-deficient mutants, GFP-tagged Sox9 plasmid and GSK-3β plasmid were subjected to site-directed mutagenesis using the inverse PCR technique. All constructs were verified by sequencing. cGKII, cGKII-Δkinase, GSK-3β$^{S9A}$, and control GFP retrovirus vectors were constructed using pMx vector and plat-E cells as described previously (42).

*Gene transfection.* For the transient transfection, a total of 1 μg plasmid DNA was transfected using Fugene6 (Roche). For cotransfection, all plasmids were added in an equal ratio. Total RNA was isolated 72 h after the transfection and used for the subsequent assays. For fluorescent detection, HeLa cells were transiently transfected, and fluorescent images were taken 24 h after transfection. To investigate the interaction of cGKII and MAPK/STAT signaling, ATDC5 cells were transfected with cGKII or the empty vector, and FGF-2 (1 ng/ml) was added 72 h after transfection. IB was then carried out using primary antibodies to p-Erk1/2, Erk1/2, p-p38MAPK, p38MAPK, p-JNK2/3, JNK2/3, p-JNK1, JNK1, p-STAT1, and STAT1 (Cell Signaling Technology) as described above.

*Real-time RT-PCR.* Total RNA was reverse-transcribed with MultiScribe RT (Applied Biosystems Inc.). Semiquantitative RT-PCR was performed within an exponential phase of the amplification, with the following primer sequences: caspase-9 forward, 5′-CGATGCAGGGTGCGCCTAGTGA-3′; caspase-9 reverse, 5′-TGACCAGCTGCCTGGCCTGATC-3′; Bad forward, 5′-CCAGGTCTCCTGGGGAGCAACATTC-3′; Bad reverse, 5′-AGCTCCTCCTCCATCCCTTCATCC-3′; PLK forward, 5′-TGGCACTCCTAACTACATAGCTCCTGAGG-3′; PLK reverse, 5′-CGGAGGTAGGTCTCTTTTAGGCACGA-3′; p90RSK forward, 5′-GATTCTTCTGCGGTATGGCCA-3′; p90RSK reverse, 5′-TGCCGTAGGATCTTATCCAGCA-3′; eNOS forward, 5′-CTCGAGTGGTTTGCTGCCCTTG-3′; eNOS reverse, 5′-CAGGTCCCTCATGCCAATCTCTGA-3′; GSK-3β forward, 5′-CCAGTATAGATGTATGGTCTG-3′; GSK-3β reverse, 5′-CTTGTTGGTGTTCCTAGG-3′; VASP forward, 5′-TTCCAGCCGGGCTACTGTGATG-3′; VASP reverse, 5′-CGGCCAACAACTCGGAAGGAGT-3′; cdc25 forward, 5′-GCACTGGAAAGGGTGGAGAGACTGG-3′; cdc25 reverse, 5′-CCTCTTCACTTGCAGGTGGGATAGG-3′; Runx2 forward, 5′-CCCAGCCACCTTTACCTACA-3′; Runx2 reverse, 5′-TATGGAGTGCTGCTGGTCTG-3′. Real-time RT-PCR was performed on an ABI 7700 Sequence Detection system (Applied Biosystems) using QuantiTect SYBR Green PCR Master Mix (Qiagen) with β-actin as the internal control and the following primer sequences: COL10 forward, 5′-CATAAAGGGCCCACTTGCTA-3′; COL10 reverse, 5′-TGGCTGATATTCCTGGTGGT-3′; ALP forward, 5′-GCTGATCATTCCCACGTTTT-3′; ALP reverse, 5′-CTGGGCCTGGTAGTTGTTGT-3′; MMP-13 forward, 5′-AGGCCTTCAGAAAAGCCTTC-3′; MMP-13 reverse, 5′-TCCTTGGAGTGATCCAGACC-3′; β-actin forward, 5′-AGATGTGGATCAGCAAGCAG-3′; β-actin reverse, 5′-GCGCAAGTTAGGTTTTGTCA-3′. All reactions were run in triplicate.

*Luciferase reporter gene assay.* The human COL10 promoter regions from −4,459 bp relative to the transcriptional start site were cloned into the pGL3-Basic vector (Promega). The TOPflash system (Upstate Biotechnology Inc.) was used according to the manufacturer's protocol. The luciferase assay was performed with a dual-luciferase reporter assay system (Promega) using a GloMax 96 Microplate Luminometer (Promega).

*IP and IB assay.* IP was performed with ProFound Myc Tag IP/Co-IP kits (Pierce) according to the manufacturer's protocol. Samples were prepared using M-PER or NE-PER (Pierce) supplemented with 2 mM $Na_3VO_4$ and 10 mM NaF according to the manufacturer's protocol. Cell lysates were incubated with the high-affinity anti-c-Myc antibody-coupled agarose

at 4°C overnight. Immunocomplexes were washed 3 times with cold wash solution. c-Myc–tagged proteins were eluted, and an equal amount of each eluted sample (15 μg) was subjected to SDS-PAGE, transferred onto nitrocellulose membranes, and subjected to IB using primary antibodies to cGKII (Santa Cruz Biotechnology Inc.), GSK-3β and Ser9-phosphorylated GSK-3β (Chemicon), and Myc tag (Upstate Biotechnology Inc.). Immunoreactive proteins were visualized as described above.

*Statistics.* Means of groups were compared by ANOVA, and significance of differences was determined by post-hoc testing by the Bonferroni method. A $P$ value less than 0.05 was considered significant.


## Acknowledgments

We thank Boris M. Hogema for providing plasmids encoding constitutively active human cGKII; Henry Kronenberg and Sakae Tanaka for critical discussions; and Reiko Yamaguchi and Mizue Ikeuchi for their excellent technical help. This work was supported by Grant-in-Aid no. 14657359 for Scientific Research from the Japanese Ministry of Education, Culture, Sports, Science and Technology.

Received for publication February 5, 2008, and accepted in revised form May 7, 2008.


Address correspondence to: Hiroshi Kawaguchi, Sensory and Motor System Medicine, Faculty of Medicine, University of Tokyo, Hongo 7-3-1, Bunkyo-ku, Tokyo 113-8655, Japan. Phone: 81-33815-5411 ext. 30473; Fax: 81-33818-4082; E-mail: kawaguchi-ort@h.u-tokyo.ac.jp.


1. Kronenberg, H.M. 2003. Developmental regulation of the growth plate. *Nature.* **423**:332–336.
2. Chusho, H., et al. 2001. Dwarfism and early death in mice lacking C-type natriuretic peptide. *Proc. Natl. Acad. Sci. U. S. A.* **98**:4016–4021.
3. Tamura, N., et al. 2004. Critical roles of the guanylyl cyclase B receptor in endochondral ossification and development of female reproductive organs. *Proc. Natl. Acad. Sci. U. S. A.* **101**:17300–17305.
4. Bartels, C.F., et al. 2004. Mutations in the transmembrane natriuretic peptide receptor NPR-B impair skeletal growth and cause acromesomelic dysplasia, type Maroteaux. *Am. J. Hum. Genet.* **75**:27–34.
5. Schulz, S. 2005. C-type natriuretic peptide and guanylyl cyclase B receptor. *Peptides.* **26**:1024–1034.
6. Pfeifer, A., et al. 1996. Intestinal secretory defects and dwarfism in mice lacking cGMP-dependent protein kinase II. *Science.* **274**:2082–2086.
7. Pfeifer, A., et al. 1999. Structure and function of cGMP-dependent protein kinases. *Rev. Physiol. Biochem. Pharmacol.* **135**:105–149.
8. Pfeifer, A., et al. 1998. Defective smooth muscle regulation in cGMP kinase I-deficient mice. *EMBO J.* **17**:3045–3051.
9. Chikuda, H., et al. 2004. Cyclic GMP-dependent protein kinase II is a molecular switch from proliferation to hypertrophic differentiation of chondrocytes. *Genes Dev.* **18**:2418–2429.
10. Doble, B.W., and Woodgett, J.R. 2003. GSK-3: tricks of the trade for a multi-tasking kinase. *J. Cell Sci.* **116**:1175–1186.
11. Holmbeck, K. 2005. Collagenase in cranial morphogenesis. *Cells Tissues Organs.* **181**:154–165.
12. Akiyama, H., Chaboissier, M.C., Martin, J.F., Schedl, A., and de Crombrugghe, B. 2002. The transcription factor Sox9 has essential roles in successive steps of the chondrocyte differentiation pathway and is required for expression of Sox5 and Sox6. *Genes Dev.* **16**:2813–2828.
13. Takeda, S., Bonnamy, J.P., Owen, M.J., Ducy, P., and Karsenty, G. 2001. Continuous expression of Cbfa1 in nonhypertrophic chondrocytes uncovers its ability to induce hypertrophic chondrocyte differentiation and partially rescues Cbfa1-deficient mice. *Genes Dev.* **15**:467–481.
14. Ornitz, D.M. 2005. FGF signaling in the developing endochondral skeleton. *Cytokine Growth Factor Rev.* **16**:205–213.
15. Yasoda, A., et al. 2004. Overexpression of CNP in chondrocytes rescues achondroplasia through a MAPK-dependent pathway. *Nat. Med.* **10**:80–86.
16. Deng, C., Wynshaw-Boris, A., Zhou, F., Kuo, A., and Leder, P. 1996. Fibroblast growth factor receptor 3 is a negative regulator of bone growth. *Cell.* **84**:911–921.
17. Hoeflich, K.P., et al. 2000. Requirement for glycogen synthase kinase-3beta in cell survival and NF-kappaB activation. *Nature.* **406**:86–90.
18. Huang, L.F., Fukai, N., Selby, P.B., Olsen, B.R., and Mundlos, S. 1997. Mouse clavicular development: analysis of wild-type and cleidocranial dysplasia mutant mice. *Dev. Dyn.* **210**:33–40.
19. Dong, Y.F., Soung do, Y., Schwarz, E.M., O'Keefe, R.J., and Drissi, H. 2006. Wnt induction of chondrocyte hypertrophy through the Runx2 transcription factor. *J. Cell Physiol.* **208**:77–86.
20. Hartmann, C., and Tabin, C.J. 2000. Dual roles of Wnt signaling during chondrogenesis in the chicken limb. *Development.* **127**:3141–3159.
21. Yano, F., et al. 2005. The canonical Wnt signaling pathway promotes chondrocyte differentiation in a Sox9-dependent manner. *Biochem. Biophys. Res. Commun.* **333**:1300–1308.
22. Tamamura, Y., et al. 2005. Developmental regulation of Wnt/beta-catenin signals is required for growth plate assembly, cartilage integrity, and endochondral ossification. *J. Biol. Chem.* **280**:19185–19195.
23. Akiyama, H., et al. 2004. Interactions between Sox9 and beta-catenin control chondrocyte differentiation. *Genes Dev.* **18**:1072–1087.
24. Schlossmann, J., and Hofmann, F. 2005. cGMP-dependent protein kinases in drug discovery. *Drug Discov. Today.* **10**:627–634.
25. Hunziker, E.B. 1994. Mechanism of longitudinal bone growth and its regulation by growth plate chondrocytes. *Microsc. Res. Tech.* **28**:505–519.
26. Wilsman, N.J., Farnum, C.E., Leiferman, E.M., Fry, M., and Barreto, C. 1996. Differential growth by growth plates as a function of multiple parameters of chondrocytic kinetics. *J. Orthop. Res.* **14**:927–936.
27. Kronenberg, H.M. 2006. PTHrP and skeletal development. *Ann. N. Y. Acad. Sci.* **1068**:1–13.
28. Pilz, R.B., and Casteel, D.E. 2003. Regulation of gene expression by cyclic GMP. *Circ. Res.* **93**:1034–1046.
29. Miyazawa, T., et al. 2002. Cyclic GMP-dependent protein kinase II plays a critical role in C-type natriuretic peptide-mediated endochondral ossification. *Endocrinology.* **143**:3604–3610.
30. Doble, B.W., Patel, S., Wood, G.A., Kockeritz, L.K., and Woodgett, J.R. 2007. Functional redundancy of GSK-3alpha and GSK-3beta in Wnt/beta-catenin signaling shown by using an allelic series of embryonic stem cell lines. *Dev. Cell.* **12**:957–971.
31. MacAulay, K., et al. 2007. Glycogen synthase kinase 3alpha-specific regulation of murine hepatic glycogen metabolism. *Cell Metab.* **6**:329–337.
32. Patel, S., Doble, B., and Woodgett, J.R. 2004. Glycogen synthase kinase-3 in insulin and Wnt signalling: a double-edged sword? *Biochem. Soc. Trans.* **32**:803–808.
33. Dominguez, I., and Green, J.B. 2001. Missing links in GSK3 regulation. *Dev. Biol.* **235**:303–313.
34. Papadopoulou, D., Bianchi, M.W., and Bourouis, M. 2004. Functional studies of shaggy/glycogen synthase kinase 3 phosphorylation sites in Drosophila melanogaster. *Mol. Cell. Biol.* **24**:4909–4919.
35. Ding, V.W., Chen, R.H., and McCormick, F. 2000. Differential regulation of glycogen synthase kinase 3beta by insulin and Wnt signaling. *J. Biol. Chem.* **275**:32475–32481.
36. Fukumoto, S., et al. 2001. Akt participation in the Wnt signaling pathway through Dishevelled. *J. Biol. Chem.* **276**:17479–17483.
37. Itaka, K., et al. 2007. Bone regeneration by regulated in vivo gene transfer using biocompatible polyplex nanomicelles. *Mol. Ther.* **15**:1655–1662.
38. Ohba, S., et al. 2007. Identification of a potent combination of osteogenic genes for bone regeneration using embryonic stem (ES) cell-based sensor. *FASEB J.* **21**:1777–1787.
39. Kamekura, S., et al. 2006. Contribution of runt-related transcription factor 2 to the pathogenesis of osteoarthritis in mice after induction of knee joint instability. *Arthritis Rheum.* **54**:2462–2470.
40. Shukunami, C., et al. 1997. Cellular hypertrophy and calcification of embryonal carcinoma-derived chondrogenic cell line ATDC5 in vitro. *J. Bone Miner. Res.* **12**:1174–1188.
41. Vaandrager, A.B., et al. 2003. Autophosphorylation of cGMP-dependent protein kinase type II. *J. Biol. Chem.* **278**:28651–28658.
42. Saito, T., Ikeda, T., Nakamura, K., Chung, U.I., and Kawaguchi, H. 2007. S100A1 and S100B, transcriptional targets of SOX trio, inhibit terminal differentiation of chondrocytes. *EMBO Rep.* **8**:504–509.

ARTHRITIS & RHEUMATISM
Vol. 58, No. 9, September 2008, pp 2764–2775
DOI 10.1002/art.23805


# The Distinct Role of the Runx Proteins in Chondrocyte Differentiation and Intervertebral Disc Degeneration

## Findings in Murine Models and in Human Disease

Shingo Sato,[1] Ayako Kimura,[1] Jerfi Ozdemir,[2] Yoshinori Asou,[1] Makiko Miyazaki,[1] Tetsuya Jinno,[1] Keisuke Ae,[1] Xiuyun Liu,[2] Mitsuhiko Osaki,[3] Yasuhiro Takeuchi,[4] Seiji Fukumoto,[5] Hiroshi Kawaguchi,[5] Hirotaka Haro,[6] Ken-ichi Shinomiya,[1] Gerard Karsenty,[2] and Shu Takeda[1]

***Objective.*** **Runx2 is a transcription factor that regulates chondrocyte differentiation. This study was undertaken to address the role of the different Runx proteins (Runx1, Runx2, or Runx3) in chondrocyte differentiation using chondrocyte-specific *Runx*–transgenic mice, and to study the importance of the QA domain of Runx2, which is involved in its transcriptional activation.**

***Methods.*** ***Runx*** **expression was analyzed in the mouse embryo by in situ hybridization. Overexpression of *Runx*1, *Runx*2 (lacking the QA domain [ΔQA]), or *Runx*3 was induced in chondrocytes in vivo, to produce α(1)II-*Runx*1, α(1)II-*Runx*2ΔQA, and α(1)II-*Runx*3 mice, respectively, for histologic and molecular analyses. Runx expression was also examined in an experimental mouse model of mechanical stress–induced intervertebral disc (IVD) degeneration and in human patients with IVD degeneration.**

***Results.*** ***Runx*1 expression was transiently observed in condensations of mesenchymal cells, whereas *Runx*2 and *Runx*3 were robustly expressed in prehypertrophic chondrocytes. Similar to α(1)II-*Runx*2 mice, α(1)II-*Runx*2ΔQA and α(1)II-*Runx*3 mice developed ectopic mineralization of cartilage, but this was less severe in the α(1)II-*Runx*2ΔQA mice. In contrast, α(1)II-*Runx*1 mice displayed no signs of ectopic mineralization. Surprisingly, α(1)II-*Runx*1 and α(1)II-*Runx*2 mice developed scoliosis due to IVD degeneration, characterized by an accumulation of extracellular matrix and ectopic chondrocyte hypertrophy. During mouse embryogenesis, Runx2, but not Runx1 or Runx3, was expressed in the IVDs. Moreover, both in the mouse model of IVD degeneration and in human patients with IVD degeneration, there was significant up-regulation of Runx2 expression.**

***Conclusion.*** **Each Runx protein has a distinct, yet overlapping, role during chondrocyte differentiation. Runx2 contributes to the pathogenesis of IVD degeneration.**

Cells of the chondrocyte lineage play critical roles at several stages of endochondral ossification (1). Chondrocytes are the first skeletal-specific cell type that can be identified in the condensations of mesenchymal cells that precede the development of skeletal elements (2).

Supported by Grant-in-Aid for Scientific Research grants from the Japan Society for the Promotion of Science to Drs. Asou, Jinno, Ae, Shinomiya, and Takeda, and by 21st Century Center of Excellence Program grants from the Ministry of Education, Culture, Sports, Science, and Technology of Japan to Drs. Shinomiya and Takeda. Dr. Takeda's work also was supported by grants from Uehara Memorial Foundation. Dr. Karsenty's work was supported by a grant from the NIH.

[1]Shingo Sato, MD, PhD, Ayako Kimura, MS, Yoshinori Asou, MD, PhD, Makiko Miyazaki, MD, Tetsuya Jinno, MD, PhD, Keisuke Ae, MD, PhD, Ken-ichi Shinomiya, MD, PhD, Shu Takeda, MD, PhD: Tokyo Medical and Dental University, Tokyo, Japan; [2]Jerfi Ozdemir, BSc, MBA, Xiuyun Liu, Gerard Karsenty, MD, PhD (current address: Columbia University, New York, New York): Baylor College of Medicine, Houston, Texas; [3]Mitsuhiko Osaki, PhD: Tottori University, Tottori, Japan; [4]Yasuhiro Takeuchi, MD, PhD: Toranomon Hospital, Tokyo, Japan; [5]Seiji Fukumoto, MD, PhD, Hiroshi Kawaguchi, MD, PhD: University of Tokyo, Tokyo, Japan; [6]Hirotaka Haro, MD, PhD: University of Yamanashi, Yamanashi, Japan.

Dr. Sato, Ms Kimura, and Ms Ozdemir contributed equally to this work.

Dr. Takeuchi has received speaking fees from Eisai Company, Ltd. and Teijin Pharma, Ltd. (less than $10,000 each).

Address correspondence and reprint requests to Shu Takeda, MD, PhD, Department of Orthopedic Surgery, Tokyo Medical and Dental University, 1-5-45 Yushima, Bunkyo-ku, Tokyo 113-8519, Japan. E-mail: shu-tky@umin.ac.jp.

Submitted for publication February 14, 2008; accepted in revised form May 29, 2008.

At these initial stages of development, chondrocytes actively divide or proliferate, and express a specific molecular marker, α1(II) collagen. Around embryonic day 14.5 of mouse development, chondrocytes in the center of these mesenchymal condensations become hypertrophic and form 2 distinct cell populations: prehypertrophic chondrocytes that continue to express α1(II) collagen, and hypertrophic chondrocytes that exit the cell cycle and express α1(X) collagen as a specific molecular marker (3). Hypertrophic chondrocytes replace the extracellular matrix with one that is permissive to vascular invasion; this allows the entry of osteoblastic cells. Subsequently, and at either end of a given skeletal element, chondrocytes organize into columns, forming growth-plate cartilage, which is responsible for linear skeletal growth (1).

Major progress has been made, over the last decade, in our understanding of the transcriptional control of chondrocyte differentiation (2). Work in multiple laboratories has established the critical role of Sox9 (4), along with Sox5 and Sox6 (5), in the differentiation of nonhypertrophic chondrocytes. Meanwhile, Runx2 (6–8), together with Runx3 (9), has been shown to favor chondrocyte hypertrophy. We previously demonstrated that continuous expression of *Runx*2 in nonhypertrophic chondrocytes (herein comprising the α(1)II-*Runx*2 group of mice) led to the development of ectopic hypertrophy of chondrocytes, followed by bone formation (7).

Runx1, the other member of the Runx family, shares a highly homologous DNA binding domain, the runt domain, with Runx2 and Runx3. There are also homologous regions N-terminal to the runt domain that are common to Runx1, Runx2, and Runx3. Although the last 5 amino acids of all 3 Runx proteins are identical, Runx2 possesses a unique QA domain composed of a stretch of Q and A residues (10).

Currently, it is unknown whether a functional hierarchy exists among Runx2, Runx3, and Runx1 (10). In addition, the significance of the QA domain of Runx2 in inducing chondrocyte differentiation remains to be elucidated. Therefore, in the present study, we generated transgenic mice that overexpressed *Runx*1 or *Runx*3 or lacked a QA domain in *Runx*2 (comprising the α(1)II-*Runx*1, α(1)II-*Runx*3, and α(1)II-*Runx*2ΔQA groups of mice, respectively). The mice were generated using the identical promoter/enhancer construct that we have previously used to specifically express *Runx*2 in chondrocytes (7).

Our results showed that all 3 *Runx* genes were expressed in cells of the chondrocyte lineage, but each functioned differently in these cells. The α(1)II-*Runx*3 and α(1)II-*Runx*2ΔQA mice developed ectopic differentiation of hypertrophic chondrocytes in chondrocostal cartilage, albeit to a lesser extent in the α(1)II-*Runx*2ΔQA mice. Surprisingly, α(1)II-*Runx*1 and α(1)II-*Runx*2 mice exhibited a kyphotic deformity of the vertebrae due to intervertebral disc (IVD) degeneration. We therefore studied an experimental mouse model of mechanical stress–induced IVD degeneration, which showed that Runx2, but not Runx1 or Runx3, was induced in the degenerated IVD. In addition, in human patients with IVD degeneration, we found that Runx2 expression was up-regulated, thus substantiating the pathophysiologic importance of Runx2 in the development of IVD degeneration in humans. This study illustrates the specific and distinct role of the *Runx* genes in physiologic conditions such as chondrocytic differentiation, and in pathologic conditions such as IVD degeneration.

## MATERIALS AND METHODS

**Generation of transgenic mice and analysis of transgene expression.** The α1(II)-*Runx*1, α1(II)-*Runx*3, and α1(II)-*Runx*2ΔQA transgenes were obtained by subcloning *Runx*1, *Runx*3, or *Runx*2ΔQA complementary DNA (cDNA) (11) into an α1(II) collagen–expressing chondrocyte–specific promoter cassette (7). Transgenic founders were obtained by pronuclear injection into C57BL/6 oocytes, as previously described (7). We thus obtained multiple lines of transgenic mice with identical phenotypes in all groups except for the α1(II)-*Runx*3 mice. The *Runx*2-deficient mice were a generous gift from Dr. M. Owen (12). Wild-type (WT) mice were purchased from Jackson Laboratories (Bar Harbor, ME).

The genotypes of the mice were determined by polymerase chain reaction (PCR). (A list of the PCR primer sequences is available upon request from the corresponding author.) Chondrocyte RNA was extracted from chondrocostal cartilage of the transgenic mouse embryos, using TRIzol (Invitrogen, Carlsbad, CA), and was then reverse-transcribed for cDNA synthesis. Expression of the transgene was analyzed quantitatively by real-time quantitative PCR (MX3000P; Stratagene, La Jolla, CA). Primers were designed against the specific poly(A) region of the transgene, which is common to all 3 transgenes, namely 5′-GCGTGCATGCGACGTCATAGCTCTC-3′ (forward) and 5′-GGTTCAGGGGGAGGTGTGGGAGG-3′ (reverse). Four mice per group were analyzed.

**Skeletal preparations.** To prepare skeletal specimens for analysis, groups of mouse skeletons were dissected at each indicated time point of development and skinned. Subsequently, the skeletons were fixed in 100% ethanol at 4°C overnight, and stained with Alcian blue dye for 1 day followed by staining with alizarin red solution according to the standard protocol (7). Specimens were cleared in 50% glycerol/50% ethanol until soft tissue staining was removed. Six mice per group were analyzed, and identical phenotypes were observed.

**Histology, in situ hybridization, and immunohistochemistry.** For histologic examination, tissue samples from the embryos were immediately fixed in 4% paraformaldehyde/phosphate buffered saline after dissection, dehydrated with gradually increasing concentrations of ethanol, and embedded

in paraffin. Tissue samples from adult mice were decalcified in 20% EDTA for 2 weeks after fixation before being embedded in paraffin. Sections were stained with 0.1% Safranin O (orange stain) to evaluate cartilage matrices, and 0.03% fast green to evaluate morphologic features, as previously described (13). In situ hybridization was performed using $^{35}$S-labeled riboprobes according to the standard protocol as described previously (7). Hybridizations were performed at 55°C.

Autoradiography and Hoechst 33528 staining were performed as previously described (7). For staining with LacZ, tails from Runx2-heterozygote mice were fixed in 0.2% paraformaldehyde at room temperature for 30 minutes, and then stained overnight in X-Gal solution as previously described (7). The following day, samples were decalcified and processed for histologic examination.

Immunohistochemistry was performed according to a standard protocol (7). Anti-Runx1 antibody (14) and anti–α1(X) collagen antibody were purchased from Santa Cruz Biotechnology (Santa Cruz, CA) and Cosmo Bio (Tokyo, Japan), respectively. The anti-Runx2 and anti-Runx3 antibodies have been described previously (7,15). Six mice per group were analyzed, and identical phenotypes were observed.

**Disc compression of mouse vertebrae and analysis of IVDs in human patients.** The vertebrae of 8-week-old female WT mice were compressed as previously described, with minor modifications (16). Briefly, the ninth and tenth caudal vertebrae were percutaneously punctured by 0.4-mm stainless steel pins and transfixed. Subsequently, the pins were instrumented using elastic springs. After 1–4 weeks, the mice were dissected and the vertebrae were examined histologically. Four mice per group were analyzed, and identical phenotypes were observed.

The study protocol involving human patients was approved by a local ethics committee. Patients with IVD degeneration were classified according to an established grading system (17). Patients with moderate disc degeneration (grade 3 to grade 4) (17) gave written informed consent for the collection of their RNA from the degenerated disc at the time of surgery. As a control, we used patients with spinal cord injury whose IVDs had no detectable damage. RNA was extracted from the IVD samples and reverse-transcribed. Expression of *Runx*2 was quantitatively analyzed by real-time quantitative PCR.

## RESULTS

**Comparison of *Runx*1, *Runx*2, and *Runx*3 expression during mouse skeletal development.** As an initial way to assess the respective contribution of each of the 3 *Runx* genes to chondrocyte differentiation, we used in situ hybridization to study their pattern of expression in the developing mouse skeletons between embryonic day 12.5 and birth. The identity of the cells expressing each *Runx* gene was determined on adjacent tissue sections using different probes, as follows: α1(I) collagen as a marker of fibroblasts and osteoblasts, α1(II) collagen as a marker of proliferating and prehypertrophic chondrocytes, α1(X) collagen as a marker of hypertrophic chondrocytes, and Indian hedgehog as a marker of prehypertrophic chondrocytes (18). This analysis was performed in vertebrae and in long bones, since chondrocyte differentiation has been extensively studied on a molecular level in both of these sites.

At embryonic day 12.5, *Runx*2 was expressed in mesenchymal cells of the perichondrium of the vertebrae (Figure 1A, arrow), but not in cells located in the vertebral body. Expression of *Runx*2 was also observed in cells of Meckel's cartilage (results not shown). These results indicate that at this stage of development, *Runx*2 was expressed in prechondrogenic cells. *Runx*1, at embryonic day 12.5, was expressed in α1(II) collagen–positive cells of the perichondrium of the vertebrae (Figure 1A, arrow), as well as in the dorsal root ganglia. In contrast, *Runx*3 expression was observed in chondrocytes in vertebral bodies (Figure 1A, arrowhead).

The chondrocytes of vertebral bodies strongly expressed Indian hedgehog (Figure 1A), suggesting that these chondrocytes were destined to become prehypertrophic. At embryonic day 14.5 and at later stages of embryonic development, *Runx*1 expression in chondrocytes was low, whereas *Runx*2 was expressed in the prehypertrophic and hypertrophic chondrocytes, and *Runx*3 was expressed in the prehypertrophic chondrocytes (Figures 1B and C and results not shown).

Results of these analyses demonstrate that all *Runx* genes are expressed at some developmental point in cells of the chondrocyte lineage. However, they have a complex and dynamic pattern of expression during chondrogenesis. These observations led us to examine the role of each of the Runx proteins in chondrogenesis.

**Generation of transgenic mice expressing *Runx*1 or *Runx*3 in nonhypertrophic chondrocytes throughout development.** We have previously shown that constitutive expression of *Runx*2 in nonhypertrophic chondrocytes resulted in premature differentiation of hypertrophic chondrocytes in long bones and in ectopic differentiation of hypertrophic chondrocytes in chondrocostal cartilage (7). The high structural similarity of the Runx proteins (Figure 2A) and their overlapping expression in chondrocytes (Figure 1) prompted us to examine the roles of Runx1 and Runx3 in chondrocyte differentiation. To accomplish this, we generated transgenic mice expressing either *Runx*1 or *Runx*3 cDNA under the control of a 3-kb–long fragment of the mouse α1(II) collagen promoter and its 3-kb–long chondrocyte-specific enhancer (19) (Figure 2A); these transgenic mice were termed α1(II)-*Runx*1 and α1(II)-*Runx*3 mice, respectively.

The expression of the transgene in α1(II)-*Runx*1 or α1(II)-*Runx*3 mice was confirmed by real-time quantitative PCR using RNA extracted from transgenic embryos. Transgene expression was restricted to the cartilage, and the expression level was

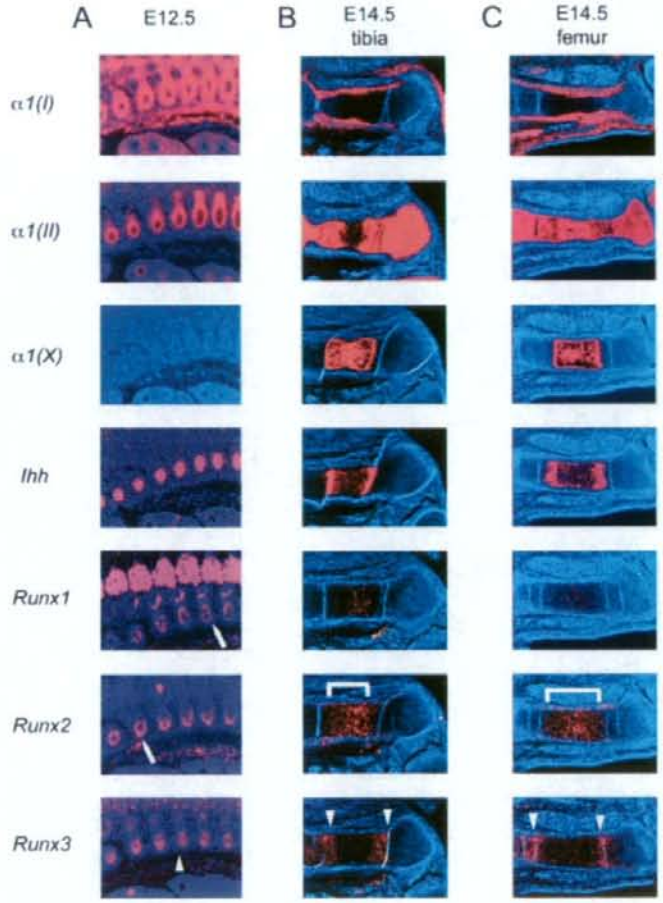


**Figure 1.** Analysis of *Runx* gene expression by in situ hybridization in the mouse vertebrae at embryonic day (E) 12.5 **(A)** and in the tibia **(B)** and femur **(C)** at embryonic day 14.5. Adjacent sections of wild-type mouse embryos were hybridized with the indicated probes. Note the expression of *Runx*1 and *Runx*2 in condensations of mesenchymal cells **(arrow) (A)**, the broad expression of *Runx*2 in nonhypertrophic chondrocytes **(bracket) (B** and **C)**, and the restricted expression of *Runx*3 in prehypertrophic chondrocytes **(arrowheads) (A–C)**. Ihh = Indian hedgehog.

comparable with that of the α1(II)-*Runx*2 transgene (Figure 2B). We obtained 2 lines for the α1(II)-*Runx*1 mice, and both lines were born at the expected Mendelian ratio and showed no overt abnormalities at birth (results not shown). In contrast, the α1(II)-*Runx*3 mice never survived until birth, and therefore analysis of these mice was performed only on skeletal preparations from transgenic embryos.

**Ectopic hypertrophic chondrocyte differentiation and endochondral ossification in α1(II)-*Runx*3 embryos, but not in α1(II)-*Runx*1 mice.** In order to study skeletal cell differentiation, we first used Alcian blue/alizarin red to stain skeletal preparations (20). Alcian blue stains were used to reveal demineralization of cartilaginous matrices, while alizarin red stains showed mineralization of cartilaginous and bony matrices.

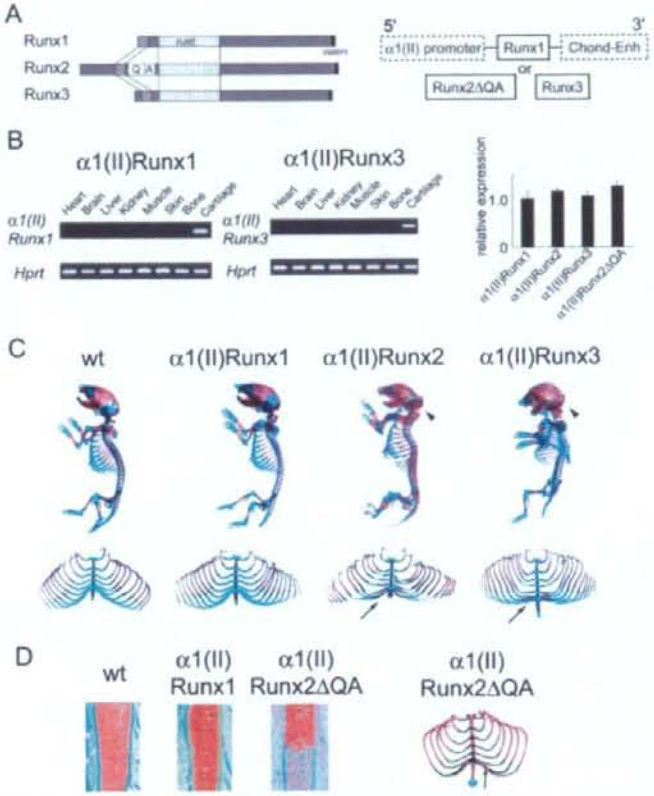


**Figure 2.** **A** and **B**, Generation of α1(II)-*Runx*–transgenic mice. **A**, Left, Comparison of the structures of the Runx proteins, which share a highly homologous runt domain. Right, Schematic representation of the construct used. Transgenic mice containing *Runx*1, *Runx*2ΔQA (lacking the QA domain of Runx2), or *Runx*3 cDNA were generated under the control of a chondrocyte-specific α1(II) collagen promoter/enhancer (Chond-Enh) cassette. **B**, Left, Cartilage-specific expression of each transgene in the α1(II)-*Runx*1 and α1(II)-*Runx*3 mice. Hypoxanthine guanine phosphoribosyltransferase (*Hprt*) amplification was used as an internal control. Right, Quantitative analysis of transgene expression by real-time polymerase chain reaction. Bars show the mean and SD relative expression. **C** and **D**, Ectopic and accelerated mineralization of cartilage in α1(II)-*Runx* mice as compared with wild-type (WT) mice. **C**, Alcian blue/alizarin red staining of skeletal preparations at birth, revealing ectopically mineralized areas in chondrocostal cartilage (**arrow**) and accelerated chondrocranium mineralization (**arrowhead**) in α1(II)-*Runx*2 and α1(II)-*Runx*3 mice, both of which were lacking in WT and α1(II)-*Runx*1 mice. **D**, Left, Histologic analysis of α1(II)-*Runx* mice by Safranin O staining of sections through chondrocostal cartilage, revealing the displacement of cartilage with bone marrow cavity in α1(II)-*Runx*2ΔQA mice, but not in α1(II)-*Runx*1 mice. Right, Alcian blue/alizarin red staining of skeletal preparations from α1(II)-*Runx*2ΔQA mice at 1 month of age, revealing the restricted appearance of ectopic mineralization (**arrow**).

The most striking phenotypic abnormality in the α1(II)-*Runx*3 embryos prebirth was ectopic calcification of the rib cage. In WT embryos, the frontal part of the rib cage, also called chondrocostal cartilage, never mineralized during development or throughout life, since chondrocyte hypertrophy does not occur in this cartilage. As a result, chondrocostal cartilage always stained blue in WT embryos (Figure 2C) and in adult mice. In contrast, the chondrocostal cartilage of α1(II)-*Runx*3 embryos stained red, indicating the existence of ectopic mineralization (Figure 2C, arrow). This phenotypic abnormality was identical to that observed in the α1(II)-*Runx*2 mice (Figure 2C, arrow), and reflected the presence of hypertrophic chondrocytes (7). However, the onset and extent of this phenotype was earlier and more severe in the α1(II)-*Runx*3 mice.

In contrast, neither the chondrocostal cartilage nor the chondrocranium ever stained red in α1(II)-

*Runx*1 mice at birth (Figure 2C). Consistent with the absence of ectopic red staining in the *Runx*1 mice at birth, histologic examination of the chondrocostal cartilage of these mutant mice failed to reveal any evidence of ectopic chondrocyte hypertrophy (Figure 2D). Therefore, these results indicate that the different Runx proteins each possess a distinct potential to induce ectopic chondrocyte hypertrophy, in which Runx2 and Runx3 can induce ectopic chondrocyte hypertrophy, whereas Runx1 cannot.

In addition to the ectopic endochondral mineralization observed, there was also premature endochondral ossification in other areas of the skeleton, such as the chondrocranium, in α1(II)-*Runx*3 and α1(II)-*Runx*2 mice (Figure 2C, arrowheads). In the α1(II)-*Runx*3 mice at birth, the chondrocranium stained red and the head circumferences were smaller, whereas the chondrocranium of the WT mice stained blue. In contrast, in the α1(II)-*Runx*1 mice at birth, the chondrocranium was never observed to be mineralized (Figure 2C).

The histologic findings in the growth plate of α1(II)-*Runx*1 mice were indistinguishable from those in the growth plate of WT mice at all stages analyzed, in the embryo and after birth (results not shown). Thus, Runx3 and Runx2, but not Runx1, possess the ability to accelerate the normal program of chondrocyte differentiation.

**Potentiation of the ability of Runx2 to induce hypertrophic chondrocyte differentiation via the Runx2 QA domain.** A unique glutamine–alanine (QA) motif is present in the amino-terminus of the runt domain of Runx2, but not in Runx1 or Runx3 (Figure 2A). In order to address the role of the QA domain in chondrocyte differentiation, we generated transgenic mice by inducing expression of a mutant form of Runx2 (11) in which the QA domain was lacking (comprising the α1(II)-*Runx*2ΔQA group of mice) (Figure 2A). Surprisingly, these mice also developed ectopic mineralization, similar to that observed in the α1(II)-*Runx*2 mice, at 1 month of age (Figure 2D), indicating that the chondrocyte differentiation ability of Runx2 does not lie solely in this domain.

Histologically, the mineralized cartilage in α1(II)-*Runx*2ΔQA mice was ectopically invaded by the bone marrow cavity (Figure 2D). However, whereas most of the male α1(II)-*Runx*2 mice died perinatally (13 of 14 transgenic mice) due to ectopic mineralization of the rib cage, none of the α1(II)-*Runx*2ΔQA mice (0 of 14 transgenic mice) died before the age of 1 month. Moreover, the extent of ectopic mineralization was significantly less severe in α1(II)-*Runx*2ΔQA mice than in α1(II)-*Runx*2 mice. These results suggest that, although the QA domain of Runx2 is not essential, it does potentiate the ability of Runx2 to differentiate chondrocytes.

**Evidence of IVD degeneration in α1(II)-*Runx*1 and α1(II)-*Runx*2 mice.** Since α1(II)-*Runx*1 mice had a normal lifespan, we investigated whether Runx1 plays other roles in the chondrocyte later in life. Surprisingly, starting at 3 months of age, 52% of the α1(II)-*Runx*1 mice (12 of 23 mice) developed kyphosis and scoliosis ($P < 0.01$ versus WT mice); by 6 months of age, all of the male and female α1(II)-*Runx*1 mice exhibited these features. In contrast, no such abnormalities were observed in WT mice. Radiographic evaluation revealed deformities of the vertebrae and IVD degeneration in the α1(II)-*Runx*1 mice (Figure 3A). This phenotype led us to analyze the integrity of the IVDs in these transgenic mice.

Histologic analysis showed that the IVDs of the WT mice were composed of 3 different tissue types: cartilaginous endplate of adjacent vertebrae bodies, outer annulus fibrosus, which is composed of dense, spatially oriented α1(I) collagen fibrils, and inner nucleus pulposus, a notochord remnant (21) that is mostly (80–90%) composed of water (Figure 3B). In the α1(II)-*Runx*1 mice, there was ectopic accumulation of extracellular matrix in the IVDs at ~3 months of age (Figure 3B), although the mice had not shown any abnormalities at 1 month of age (results not shown). In addition, Schmorl's node, an abnormal herniation of fibrocartilaginous tissue through the endplate and, thus, a hallmark of endplate degeneration, was also observed in α1(II)-*Runx*1 mice at 3 months of age (Figure 3D, arrow). At 6 months of age, the organized structure of the annulus fibrosus was lost, and the inner nucleus was totally replaced by extracellular matrices and had become dehydrated (Figure 3B, arrow). Also, clusters of hypertrophic chondrocytes stained positive by immunohistochemistry for α1(X) collagen (Figure 3C, arrow), although this had never been observed in the WT mice.

To determine whether this was a specific feature of Runx1 or whether other Runx proteins could also affect the integrity of the IVD later in life, we analyzed adult α1(II)-*Runx*2 mice. Similar to that observed in the α1(II)-*Runx*1 mice, the α1(II)-*Runx*2 mice that survived perinatally also developed IVD degeneration by 3 months of age (Figures 3A and B, arrow). Histologically, there was ectopic differentiation of hypertrophic chondrocytes in the IVDs of the α1(II)-*Runx*2 mice (Figure 3C, arrow), as was observed in the α1(II)-*Runx*1 mice. Collectively, these results indicate that when the Runx proteins are overexpressed, they can affect IVD integrity.

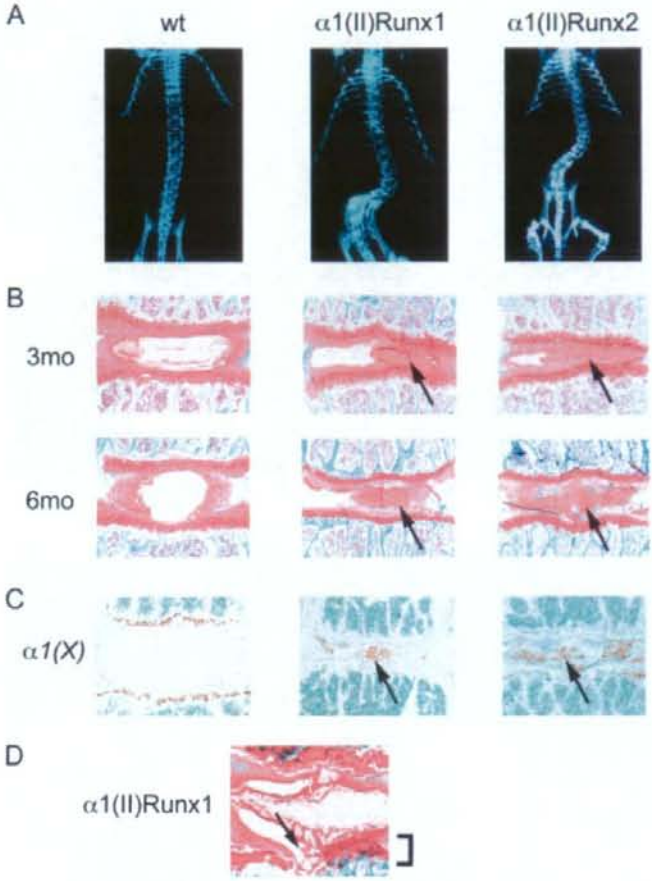


**Figure 3.** Intervertebral disc (IVD) degeneration in α1(II)-*Runx*1 and α1(II)-*Runx*2 mice. **A,** Radiographic analysis of the vertebrae at 3 months revealed marked scoliosis in the IVDs of α1(II)-*Runx* mice as compared with wild-type (WT) mice. **B–D,** Coronally cut sections of the IVDs, along with adjacent vertebral bodies, were assessed histologically by Safranin O staining (**B** and **D**), and by immunohistochemistry (**C**), which showed ectopic α1(X) collagen expression. Note the progressive degeneration of the IVDs and displacement by extracellular matrix in the α1(II)-*Runx*1 and α1(II)-*Runx*2 mice (**arrow**) (**B** and **C**), and the protrusion of the IVD (**arrow**) through the endplate into the columnar growth plate (**bracket**) in α1(II)-*Runx*1 mice (**D**).

**Induction of *Runx* gene expression in the cartilaginous endplate following weight loading.** The fact that there were phenotypic abnormalities in adult α1(II)-*Runx*1 and α1(II)-*Runx*2 mice suggested that the Runx proteins may have an as yet unappreciated function in the IVD. To address this question, we first analyzed the expression of *Runx* genes in IVDs during embryonic development. At embryonic day 16.5, all of the *Runx* genes were expressed in specific regions of the vertebral body and/or the IVD (Figure 4A). *Runx*1 was mainly expressed in the primary ossification center. *Runx*2 was also expressed in the ossification center, in chondrocytes and cells surrounding the prospective IVD. *Runx*3 was specifically expressed in prehypertrophic chondrocytes.

We also analyzed the expression of each Runx protein by immunohistochemistry, which revealed identical patterns of expression between the 3 proteins

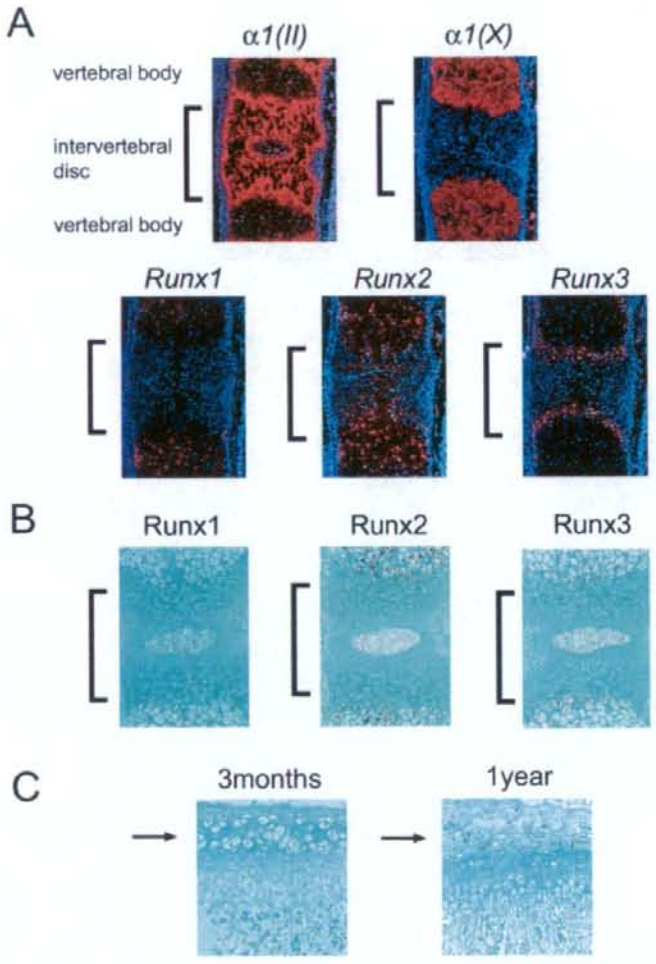


**Figure 4.** Expression of *Runx*2 in intervertebral discs (IVDs). Adjacent sections of wild-type mouse embryos at embronic day 16.5 were assessed by in situ hybridization using the indicated probes **(A)**, and by immunohistochemical analysis **(B** and **C)**. Note the expression of *Runx*2 in the prospective IVD **(bracket)** (**A** and **B**). Immunohistochemical analysis of the IVDs after birth revealed that *Runx*2 was not expressed in the wild-type mice at 3 months of age, but was expressed at 1 year **(arrow)** (**C**).

(Figure 4B). These analyses showed that Runx2 was the only member of the family that was physiologically expressed in the prospective IVD.

We next analyzed *Runx*2 expression in the IVDs of WT mice after birth. Whereas the expression of *Runx*2 in the IVDs was close to background values at 1 month and 3 months of age (results not shown and Figure 4C), it had increased in the endplate of the IVDs of WT mice at 1 year (Figure 4C, arrow).

Since the overexpression of *Runx*1 or *Runx*2 led to degeneration of the IVD, and Runx2 protein was detected in the IVD, we tested whether *Runx*1 or *Runx*2 induces IVD degradation in pathologic conditions. To test this possibility, we analyzed the biomechanical func-

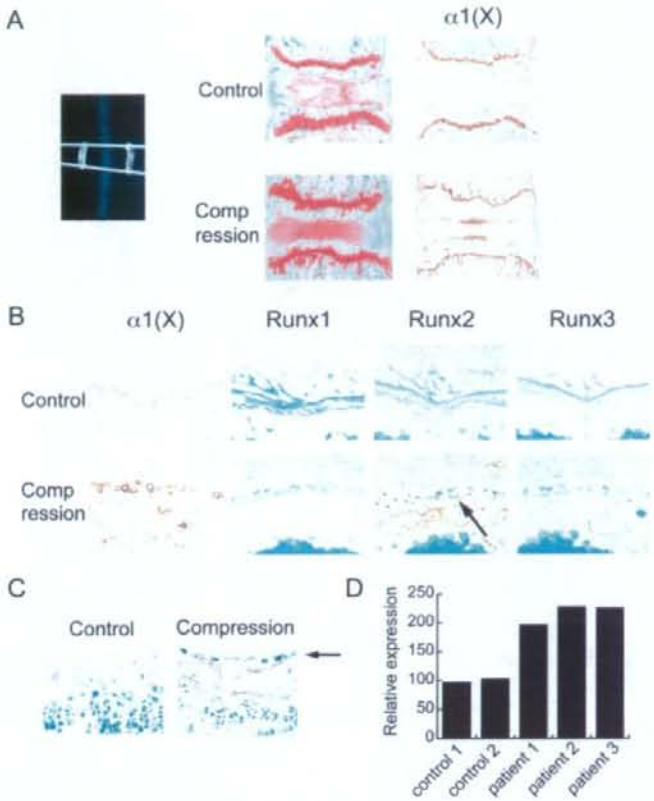


**Figure 5.** Evaluation of intervertebral disc (IVD) degeneration in mice and humans. **A,** Induction of *Runx*2 expression by mechanical compression in a mouse model of IVD degeneration. Caudal vertebrae from 2-month-old wild-type mice were compressed by an elastic spring, and then assessed by radiography (left), histology (middle), and immunohistochemistry (with Safranin O staining) (right). The compressed IVDs showed degeneration and ectopic α1(X) collagen expression (right). **B,** Immunohistochemical analysis of the expression of Runx proteins in adjacent sections of the compressed vertebrae. Note the specific induction of Runx2 in the endplate of the compressed vertebrae (**arrow**), with coexpression of α1(X) collagen. **C,** Induction of *Runx*2 mRNA expression by compression. Vertebrae from *Runx*2$^{+/-}$ mice were compressed and analyzed by LacZ staining. Note the specific induction of *Runx*2 mRNA in the endplate (**arrow**). **D,** Up-regulation of *Runx*2 in human patients with IVD degeneration. Quantitative polymerase chain reaction showed that *Runx*2 expression was significantly up-regulated in patients with IVD degeneration compared with unaffected control subjects.

tion of the IVDs of WT mice in a model of mechanical stress–induced compression, the most frequent cause of IVD degeneration. For this test, we transfixed the vertebral body with steel wire and instrumenting elastics for 4 weeks (Figure 5A), and compared Runx protein accumulation before and after compression.

After compression of the IVDs, typical disc degeneration was observed, in the form of a damaged endplate and massive induction of cells positive for type X collagen, which indicated the appearance of hypertrophic chondrocytes (Figure 5A). *Runx*1 expression was undetectable before and after compression (Figure 5B), suggesting that *Runx*1 does not contribute to IVD degeneration under these conditions. *Runx*3 expression was observed after compression, albeit at a very low level (Figure 5B). In sharp contrast, there was strong induction of Runx2 protein expression in the endplate after compression (Figure 5B, arrow). Moreover, cells expressing Runx2 also expressed α1(X) collagen, indicative of the appearance of hypertrophic chondrocytes (Figure 5B).

We took advantage of the LacZ allele that was inserted in the *Runx*2 locus in *Runx*2$^{+/-}$ mice. *Runx*2 messenger RNA (mRNA) expression can be monitored by LacZ staining in these mice. Before compression, we were able to observe *Runx*2 mRNA expression in osteoblasts on bone trabeculae and growth-plate chondrocytes, but not in the endplate, demonstrating that expression of *Runx*2 was minimal. Surprisingly, after compression, numerous LacZ-positive cells were observed in the cartilaginous endplate (Figure 5C), thus demonstrating that compression induced *Runx*2 expression.

**Up-regulation of Runx2 in human IVD degeneration.** Finally, to determine if the induction of Runx2 is also involved in the development of IVD degeneration in humans, we analyzed *Runx*2 mRNA expression in patients with moderate disc degeneration. We collected RNA from the affected IVDs of these patients, and compared the RNA levels with those in intact IVDs as a control. Similar to that observed in the mouse model, expression of *Runx*2 mRNA was up-regulated in all patients with IVD degeneration examined (Figure 5D). Taken together, these results clearly demonstrate that in both mice and humans, IVD degeneration is accompanied by induction of Runx2.

## DISCUSSION

On the basis of previous findings showing that Runx2 is an important regulator of chondrocyte hypertrophy, we examined the role of other Runx family members, Runx1 and Runx3, in chondrocytes, particularly in chondrocyte differentiation in vivo, and compared these results with those obtained for Runx2. Overexpression of *Runx*1, *Runx*2, or *Runx*3 in nonhypertrophic chondrocytes led to skeletal abnormalities, indicating that the expression of these genes at precise times during skeletal development and chondrocyte differentiation is important, and that each gene must have a distinct role in the differentiation of chondrocytes.

In addition to the ectopic mineralization observed, overexpression of *Runx*1 or *Runx*2 led to IVD degeneration. We showed that Runx2 is the only family member normally expressed in the IVD, and that Runx2 expression, along with chondrocyte hypertrophy, were induced in a mouse model of IVD degeneration. Finally, we demonstrated that in human patients with IVD degeneration, Runx2 expression was significantly up-regulated, thus suggesting that Runx2 contributes to the pathogenesis of IVD degeneration through the induction of chondrocyte hypertrophy.

In the present study, *Runx*1 expression in WT mice was restricted mostly to progenitor cells that were not yet committed to either the chondrocyte or the osteoblast lineage, a finding consistent with that described in other reports (22,23). Overexpression of *Runx*1 in chondrocytes does not induce any phenotypic abnormalities in the growth-plate chondrocyte, suggesting that Runx1 does not play a major role in the differentiation of these chondrocytes. Interestingly, it has been reported that forced expression of *Runx*1 in mesenchymal cells induced chondrocyte differentiation in vitro (24). This indicates that the function of Runx1 is possibly required only in the very early stages of chondrocyte differentiation. However, because the present study used an $\alpha$1(II) collagen promoter to drive *Runx*1 expression, and this promoter is active only in cells that have differentiated into chondrocytes, we were precluded from testing this possibility.

Our results also showed that in WT mice, *Runx*3 was expressed in prehypertrophic chondrocytes and, in contrast to *Runx*2, its expression did not decrease throughout embryonic development, suggesting that *Runx*3 may play a role in chondrocyte differentiation after birth (8,9). Previously, Runx3, in conjunction with Runx2, was shown to regulate chondrocyte differentiation, but the neonatal mortality of Runx3-deficient mice hampered any further study of the role of Runx3 in the postnatal period (9). We recently observed that Runx3-deficient mice that survived perinatally exhibited impaired longitudinal growth postnatally (Takeda S, et al: unpublished observations). This observation, together with the ectopic mineralization in $\alpha$1(II)-*Runx*3 mice, substantiates the physiologic importance of Runx3 in chondrocyte differentiation.

The results from the present study also showed that each member of the Runx family has a distinct ability to drive chondrocyte differentiation in vivo. Notably, only the $\alpha$1(II)-*Runx*2 mice developed the phenotypes of both ectopic mineralization and IVD degeneration. This ability of Runx2 to induce both intervertebral degeneration and growth-plate chondrocyte differentiation could be attributable to its unique expression pattern or to its ability to recruit specific coregulators. The latter explanation is more likely, since the Runx-transgenic mice had distinct phenotypes despite comparable patterns of expression and comparable levels of each transgene driven by the same promoter cassette in each mouse. Since the runt DNA binding domain was observed to be highly homologous with that in other Runx proteins (Figure 2A), and yet the $\alpha$1(II)-*Runx*2$\Delta$QA mice still exhibited ectopic chondrocyte differentiation (Figure 2D), it is conceivable that the carboxyl domain

of Runx2 may interact with specific coregulators to induce chondrocyte differentiation.

Indeed, many transcriptional regulators have been found to be associated with the C-terminus of Runx2 (25–29). Of these regulators, Smad3 is the most promising, since Runx2, but not Runx1 or Runx3, has been shown to induce osteocalcin promoter activity, and this was inhibited by activation of transforming growth factor $\beta$ (TGF$\beta$) or Smad3 (30,31). Moreover, mice that either expressed a dominant-negative form of the TGF$\beta$II receptor or were deficient in Smad3 developed accelerated chondrocyte differentiation as well as kyphosis (32,33), which is reminiscent of the phenotype observed in $\alpha$1(II)-*Runx*2 mice. Therefore, TGF$\beta$/Smad3 signaling and Runx2 may cooperatively regulate chondrocyte differentiation. This hypothesis would be supported if Runx2 activity were shown to be increased either in mice expressing a dominant-negative form of the TGF$\beta$II receptor or in mice deficient in Smad3.

The most interesting and unexpected finding in the present study was the observation of IVD degeneration in both $\alpha$1(II)-*Runx*1 and $\alpha$1(II)-*Runx*2 mice. IVD degeneration is one of the most common degenerative disorders of the joints (34). Although matrix metalloproteinase 3 and a number of matrix genes, such as type II collagen, type IX collagen, and aggrecan, have been shown to be involved in the pathogenesis of IVD degeneration, the molecular mechanism is still largely unknown.

In this study, we demonstrated that Runx2 is involved in the development of IVD degeneration. There was substantial evidence to support this conclusion. First, overexpression of *Runx*2 or *Runx*1 in cartilaginous endplates induced IVD destruction. Second, weight loading, which is clinically a major cause of IVD degradation, induced expression of *Runx*2, but not that of *Runx*1, in the endplate of WT mice. Third, *Runx*2 expression coincided with the region of degradation of extracellular matrices in WT mice. We showed that Runx2 protein was expressed in older WT mice, but not in young mice; this coincided with the timeframe over which some of the WT mice developed IVD degradation. Finally, *Runx*2 expression was clearly induced in the degraded IVD in human patients.

Notably, the phenotypic abnormalities observed in $\alpha$1(II)-*Runx*1– or $\alpha$1(II)-*Runx*2–transgenic mice did not completely recapitulate the phenotype observed in human patients with IVD degeneration. Nevertheless, although the phenotype was much milder in mice with mechanical stress–induced IVD degeneration, it still led to concurrent expression of *Runx*2 in the mice. In fact, histologically, these mice exhibited degenerated nucleus pulposus without IVD height abnormalities, equivalent to the grade 3 to grade 4 IVD degeneration (17) observed in human patients. Collectively, our observations in mice and humans strongly support the hypothesis that Runx2 is intimately involved in IVD degradation and may even physiologically initiate the process.

The molecular mechanism by which mechanical loading induces expression of Runx2 in the IVD is unknown. However, it has been reported that mechanical loading induces Runx2 expression in osteoblasts through the MAP kinase pathway (35), and this same pathway may also be involved in the Runx2 expression observed in IVD degeneration. Given the prevalence of IVD degeneration in humans, an approach involving manipulation of the activity or expression of *Runx*2 or its downstream genes may be an attractive proposition as a novel therapy for these types of conditions.

## ACKNOWLEDGMENTS

We would like to thank M. Patel, T. Kato, M. Noda, and U. Chung for helpful discussions and for reading the text. We also thank S. Sunamura and J. Chen for their superb technical assistance, and B. de Crombrugghe for providing the $\alpha$1(II) collagen promoter and enhancer cassette.

## AUTHOR CONTRIBUTIONS

Dr. Takeda had full access to all of the data in the study and takes responsibility for the integrity of the data and the accuracy of the data analysis.

**Study design.** Takeda.

**Acquisition of data.** Sato, Kimura, Ozdemir, Asou, Miyazaki, Jinno, Ae, Liu, Osaki, Takeuchi, Fukumoto, Kawaguchi, Haro, Shinomiya, Karsenty.

**Analysis and interpretation of data.** Takeda.

**Manuscript preparation.** Takeda.

**Statistical analysis.** Takeda.

## REFERENCES

1. Kronenberg HM. Developmental regulation of the growth plate. Nature 2003;423:332–6.
2. Karsenty G, Wagner EF. Reaching a genetic and molecular understanding of skeletal development [review]. Dev Cell 2002;2: 389–406.
3. Poole AR. The growth plate: cellular physiology, cartilage assembly and mineralization. In: Hall BK, Newman SA, editors. Cartilage: molecular aspects. Boca Raton (FL): CRC Press; 1991. p. 179–211.
4. Bi W, Deng JM, Zhang Z, Behringer RR, de Crombrugghe B. Sox9 is required for cartilage formation. Nat Genet 1999;22:85–9.
5. Akiyama H, Chaboissier MC, Martin JF, Schedl A, de Crombrugghe B. The transcription factor Sox9 has essential roles in successive steps of the chondrocyte differentiation pathway and is required for expression of Sox5 and Sox6. Genes Dev 2002;16: 2813–28.
6. Ueta C, Iwamoto M, Kanatani N, Yoshida C, Liu Y, Enomoto-Iwamoto M, et al. Skeletal malformations caused by overexpres-

sion of Cbfa1 or its dominant negative form in chondrocytes. J Cell Biol 2001;153:87–100.
7. Takeda S, Bonnamy JP, Owen MJ, Ducy P, Karsenty G. Continuous expression of Cbfa1 in nonhypertrophic chondrocytes uncovers its ability to induce hypertrophic chondrocyte differentiation and partially rescues Cbfa1-deficient mice. Genes Dev 2001;15: 467–81.
8. Stricker S, Fundele R, Vortkamp A, Mundlos S. Role of Runx genes in chondrocyte differentiation. Dev Biol 2002;245:95–108.
9. Yoshida CA, Yamamoto H, Fujita T, Furuichi T, Ito K, Inoue K, et al. Runx2 and Runx3 are essential for chondrocyte maturation, and Runx2 regulates limb growth through induction of Indian hedgehog. Genes Dev 2004;18:952–63.
10. Ito Y, Miyazono K. RUNX transcription factors as key targets of TGF-β superfamily signaling. Curr Opin Genet Dev 2003;13:43–7.
11. Thirunavukkararsu K, Mahajan M, McLarren KW, Stifani S, Karsenty G. Two domains unique to the osteoblast-specific transcription factor Osf2/Cbfa1 contribute to its transactivation function and its inability to heterodimerize with Cbfβ. Mol Cell Biol 1998;18:4197–208.
12. Otto F, Thornell AP, Crompton T, Denzel A, Gilmour KC, Rosewell IR, et al. Cbfa1, a candidate gene for cleidocranial dysplasia syndrome, is essential for osteoblast differentiation and bone development. Cell 1997;89:765–71.
13. Van der Kraan PM, Vitters EL, van Beuningen HM, van de Putte LB, van den Berg WB. Degenerative knee joint lesions in mice after a single intra-articular collagenase injection: a new model of osteoarthritis. J Exp Pathol (Oxford) 1990;71:19–31.
14. Planaguma J, Diaz-Fuertes M, Gil-Moreno A, Abal M, Monge M, Garcia A, et al. A differential gene expression profile reveals overexpression of RUNX1/AML1 in invasive endometrioid carcinoma. Cancer Res 2004;64:8846–53.
15. Osaki M, Moriyama M, Adachi K, Nakada C, Takeda A, Inoue Y, et al. Expression of RUNX3 protein in human gastric mucosa, intestinal metaplasia and carcinoma. Eur J Clin Invest 2004;34: 605–12.
16. Lotz JC, Colliou OK, Chin JR, Duncan NA, Liebenberg E. Compression-induced degeneration of the intervertebral disc: an in vivo mouse model and finite-element study. Spine 1998;23: 2493–506.
17. Pfirrmann CW, Metzdorf A, Zanetti M, Hodler J, Boos N. Magnetic resonance classification of lumbar intervertebral disc degeneration. Spine 2001;26:1873–8.
18. Mundlos S. Expression patterns of matrix genes during human skeletal development. Prog Histochem Cytochem 1994;28:1–47.
19. Zhou G, Lefebvre V, Zhang Z, Eberspaecher H, de Crombrugghe B. Three high mobility group-like sequences within a 48-base pair enhancer of the Col2a1 gene are required for cartilage-specific expression in vivo. J Biol Chem 1998;273:14989–97.
20. McLeod MJ. Differential staining of cartilage and bone in whole mouse fetuses by alcian blue and alizarin red S. Teratology 1980;22:299–301.
21. Urban JP, Roberts S. Degeneration of the intervertebral disc. Arthritis Res Ther 2003;5:120–30.
22. Smith N, Dong Y, Lian JB, Pratap J, Kingsley PD, van Wijnen AJ, et al. Overlapping expression of Runx1(Cbfa2) and Runx2(Cbfa1) transcription factors supports cooperative induction of skeletal development. J Cell Physiol 2005;203:133–43.
23. Yamashiro T, Aberg T, Levanon D, Groner Y, Thesleff I. Expression of Runx1, -2 and -3 during tooth, palate and craniofacial bone development. Mech Dev 2002;119 Suppl 1:S107–10.
24. Wang Y, Belflower RM, Dong YF, Schwarz EM, O'Keefe RJ, Drissi H. Runx1/AML1/Cbfa2 mediates onset of mesenchymal cell differentiation toward chondrogenesis. J Bone Miner Res 2005;20: 1624–36.
25. Xiao G, Jiang D, Ge C, Zhao Z, Lai Y, Boules H, et al. Cooperative interactions between activating transcription factor 4 and Runx2/Cbfa1 stimulate osteoblast-specific osteocalcin gene expression. J Biol Chem 2005;280:30689–96.
26. Wang W, Wang YG, Reginato AM, Glotzer DJ, Fukai N, Plotkina S, et al. Groucho homologue Grg5 interacts with the transcription factor Runx2-Cbfa1 and modulates its activity during postnatal growth in mice. Dev Biol 2004;270:364–81.
27. Gutierrez S, Javed A, Tennant DK, van Rees M, Montecino M, Stein GS, et al. CCAAT/enhancer-binding proteins (C/EBP) β and δ activate osteocalcin gene transcription and synergize with Runx2 at the C/EBP element to regulate bone-specific expression. J Biol Chem 2002;277:1316–23.
28. Thomas DM, Carty SA, Piscopo DM, Lee JS, Wang WF, Forrester WC, et al. The retinoblastoma protein acts as a transcriptional coactivator required for osteogenic differentiation. Mol Cell 2001; 8:303–16.
29. Zhang YW, Yasui N, Ito K, Huang G, Fujii M, Hanai J, et al. A RUNX2/PEBP2α A/CBFA1 mutation displaying impaired transactivation and Smad interaction in cleidocranial dysplasia. Proc Natl Acad Sci U S A 2000;97:10549–54.
30. Alliston T, Choy L, Ducy P, Karsenty G, Derynck R. TGF-β-induced repression of CBFA1 by Smad3 decreases cbfa1 and osteocalcin expression and inhibits osteoblast differentiation. EMBO J 2001;20:2254–72.
31. Kang JS, Alliston T, Delston R, Derynck R. Repression of Runx2 function by TGF-β through recruitment of class II histone deacetylases by Smad3. EMBO J 2005;24:2543–55.
32. Serra R, Johnson M, Filvaroff EH, LaBorde J, Sheehan DM, Derynck R, et al. Expression of a truncated, kinase-defective TGF-β type II receptor in mouse skeletal tissue promotes terminal chondrocyte differentiation and osteoarthritis. J Cell Biol 1997; 139:541–52.
33. Yang X, Chen L, Xu X, Li C, Huang C, Deng CX. TGF-β/Smad3 signals repress chondrocyte hypertrophic differentiation and are required for maintaining articular cartilage. J Cell Biol 2001;153: 35–46.
34. Powell MC, Wilson M, Szypryt P, Symonds EM, Worthington BS. Prevalence of lumbar disc degeneration observed by magnetic resonance in symptomless women. Lancet 1986;2:1366–7.
35. Ziros PG, Gil AP, Georgakopoulos T, Habeos I, Kletsas D, Basdra EK, et al. The bone-specific transcriptional regulator Cbfa1 is a target of mechanical signals in osteoblastic cells. J Biol Chem 2002;277:23934–41.

THE JOURNAL OF BIOLOGICAL CHEMISTRY VOL. 283, NO. 36, pp. 24682–24689, September 5, 2008


# Krüppel-like Factor 5 Causes Cartilage Degradation through Transactivation of Matrix Metalloproteinase 9*[S]

Received for publication, December 3, 2007, and in revised form, June 23, 2008 Published, JBC Papers in Press, July 10, 2008, DOI 10.1074/jbc.M709857200

**Yusuke Shinoda[‡], Naoshi Ogata[§], Akiro Higashikawa[‡], Ichiro Manabe[¶], Takayuki Shindo[¶], Takashi Yamada[‡], Fumitaka Kugimiya[‡], Toshiyuki Ikeda[§], Naohiro Kawamura[‡], Yosuke Kawasaki[‡], Kensuke Tsushima[¶], Norifumi Takeda[¶], Ryozo Nagai[¶], Kazuto Hoshi[‡], Kozo Nakamura[‡], Ung-il Chung[§], and Hiroshi Kawaguchi[‡1]**

*From [‡]Sensory and Motor System Medicine, [¶]Circulatory Medicine, and [§]Bone and Cartilage Regeneration Medicine, University of Tokyo, Tokyo 113-8655, Japan*

**Although degradation of cartilage matrix has been suggested to be a rate-limiting step for endochondral ossification during skeletal development, little is known about the transcriptional regulation. This study investigated the involvement of KLF5 (Krüppel-like factor 5), an Sp/KLF family member, in the skeletal development. KLF5 was expressed in chondrocytes and osteoblasts but not in osteoclasts. The heterozygous deficient ($KLF5^{+/-}$) mice exhibited skeletal growth retardation in the perinatal period. Although chondrocyte proliferation and differentiation were normal, cartilage matrix degradation was impaired in $KLF5^{+/-}$ mice, causing delay in replacement of cartilage with bone at the primary ossification center in the embryonic limbs and elongation of hypertrophic chondrocyte layer in the neonatal growth plates. Microarray analyses identified MMP9 (matrix metalloproteinase 9) as a transcriptional target, since it was strongly up-regulated by adenoviral transfection of KLF5 in chondrogenic cell line OUMS27. The KLF5 overexpression caused gelatin degradation by stimulating promoter activity of MMP9 without affecting chondrocyte differentiation or vascular endothelial growth factor expression in the culture of chondrogenic cells; however, in osteoclast precursors, it affected neither MMP9 expression nor osteoclastic differentiation. KLF5 dysfunction by genetic heterodeficiency or RNA interference was confirmed to cause reduction of MMP9 expression in cultured chondrogenic cells. MMP9 expression was decreased in the limbs of $KLF5^{+/-}$ embryos, which was correlated with suppression of matrix degradation, calcification, and vascularization. We conclude that KLF5 causes cartilage matrix degradation through transcriptional induction of MMP9, providing the first evidence that transcriptional regulation of a proteinase contributes to endochondral ossification and skeletal development.**

Endochondral ossification is an essential process for skeletal development and growth (1). During the process, chondrocytes undergo proliferation and hypertrophic differentiation. The hypertrophic chondrocytes then secrete a specialized extracellular matrix rich in type X collagen (COL10),[2] which is replaced by bone matrix. The ossification begins with chondrocyte apoptosis, cartilage matrix degradation, calcification, vascular invasion from perichondrium and bone marrow, and deposition of bone matrix by osteoblasts (2). Among these individual steps, previous studies have indicated that degradation of cartilage matrix is particularly crucial (3–6). This step requires proteolytic breakdown by a variety of proteinases, among which members of the matrix metalloproteinase (MMP) family are of special interest due to their ability to cleave collagens and aggrecan, the two principal matrix components of cartilage (7, 8). However, little is known about transcriptional regulation of MMPs in the endochondral ossification process.

Members of the Krüppel-like factor (KLF) family are important transcription factors that regulate development, cellular differentiation and growth, and pathogenesis of atherosclerosis and tumor development, by controlling the expression of a large number of genes with GC/GT-rich promoters (9). There are currently 17 known members of the mammalian KLF family (10), each of which has individually important biological functions (11). Among the members, KLF5 (IKLF, BTEB2) was identified as a positive regulator of SMemb, a marker gene for activated smooth muscle cells in vascular disease (12). KLF5 shows temporal changes in expression during embryogenesis, with diverse functions in cell differentiation and embryonic development (13, 14). Although KLF5 homozygous knock-out ($KLF5^{-/-}$) mice die *in utero* before embryonic day 8.5 (E8.5), the heterozygous knock-out ($KLF5^{+/-}$) mice are apparently normal and fertile (15). Further analyses of these mice revealed that KLF5 mediates cardiovascular remodeling, since the mice exhibited attenuated cardiac hypertrophy and fibrosis as well as much less granulation formation in response to vascular injury (15). The neonatal $KLF5^{+/-}$ mice also exhibited a marked deficiency in white adipose tissue development, suggesting a contribution to adipogenesis (16).

The KLF family shares similar zinc finger structures with the Sp family, some members of which are known to be essential for

* This work was supported by Grants-in-aid for Scientific Research 16659401 and 18209047 from the Japanese Ministry of Education, Culture, Sports, Science, and Technology. The costs of publication of this article were defrayed in part by the payment of page charges. This article must therefore be hereby marked "*advertisement*" in accordance with 18 U.S.C. Section 1734 solely to indicate this fact.

[S] The on-line version of this article (available at http://www.jbc.org) contains supplemental Tables 1 and 2 and Figs. 1–5.

[1] To whom correspondence should be addressed. Tel.: 81-33815-5411 (ext. 30473); Fax: 81-33818-4082; E-mail: kawaguchi-ort@h.u-tokyo.ac.jp.

[2] The abbreviations used are: COL10, type X collagen; COL2, type II collagen; KLF, Krüppel-like factor; M-CSF, macrophage-colony stimulation factor; M-BMMΦ, M-CSF dependent-bone marrow macrophages; MMP, matrix metalloproteinase; TRAP, tartrate-resistant acid phosphate; RANKL, receptor activator of nuclear factor κB ligand; HE, hematoxylin and eosin; TUNEL, terminal dUTP nick-end labeling; EV, empty vector; RT, reverse transcription; VEGFA, vascular endothelial growth factor A; *En*, embryonic day *n*; ADAMTS, a disintegrin and metalloproteinase with thrombospondin-like repeat.

skeletal development and growth. For example, Sp3 and Sp7 (osterix) are required for skeletal ossification (17) and osteoblast differentiation (18), respectively. The present study initially detected KLF5 expression in cells of bone and cartilage. To learn the role of KLF5, we analyzed the skeleton of KLF5$^{+/-}$ mice and found that the KLF5 insufficiency caused impaired degradation of cartilage matrix in the perinatal period. We further investigated the underlying molecular mechanisms.

## EXPERIMENTAL PROCEDURES

*Mice*—Generation of KLF5$^{+/-}$ mice was described previously (15). All mice were maintained in the C57BL/6 background with a standard diet. In each experiment, male mice of KLF5$^{+/-}$ and the wild-type littermates were compared. All experiments were performed according to the protocol approved by the Animal Care and Use Committee of the University of Tokyo.

*Cell Cultures*—Mouse osteoblastic cell line MC3T3-E1, mouse chondrogenic cell line ATDC5, and mouse monocyte-macrophagic cell line RAW264.7 were purchased from RIKEN. Human chondrogenic cell line OUMS27 was purchased from the Health Science Research Resources Bank. For isolation of primary osteoblasts, calvariae of neonatal wild-type mice were digested for 10 min at 37 °C in an enzyme solution containing 0.1% collagenase and 0.2% dispase five times, and cells isolated by the last four digestions were combined. Primary chondrocytes were prepared from ventral rib cages (excluding the sternum) of E18.5 wild-type mouse embryos as previously described (19). For mature osteoclasts, macrophage colony-stimulating factor (M-CSF)-dependent bone marrow macrophages (M-BMMΦ), which are known to be osteoclast precursors, were isolated from bone marrow of 6–8-week-old mice, as previously described (20), and cultured in the presence of M-CSF (30 ng/ml) and soluble receptor activator of nuclear factor κB ligand (RANKL; 100 ng/ml) for 3 days. Primary osteoblasts and MC3T3-E1 cells were cultured in α-minimal essential medium containing 10% fetal bovine serum. Primary chondrocytes, ATDC5, OUMS27, and Raw264.7 cells were cultured in Dulbecco's modified Eagle's medium containing 10% FBS. For proliferation assay of primary chondrocytes, cell number was counted using Cell Counting Kit-8 (Dojindo).

*Histological Analyses*—The whole skeletons of wild-type and KLF5$^{+/-}$ littermate embryos (E16.5) were fixed in 99.5% ethanol, transferred to acetone, and stained in a solution containing Alizarin red S and Alcian blue 8GX (Sigma). Tibial limbs were fixed in 4% paraformaldehyde/PBS, embedded in paraffin, sectioned in 5-μm slices, and stained with hematoxylin and eosin (HE), toluidine blue, Safranin-O, and 5% silver nitrate (von Kossa), according to the standard procedures. TUNEL staining was performed using an apoptosis *in situ* detection kit (Wako), according to the manufacturer's instruction. TRAP-positive cells were stained at pH 5.0 in the presence of L-(+)-tartaric acid using naphthol AS-MX phosphate in *N,N*-dimethyl formamide as the substrate. For immunohistochemistry, rabbit anti-mouse antibodies against KLF5 (1:100; KM1785) (15), type II collagen (COL2) (1:1000; LSL), COL10 (1:1000; LSL), and osteopontin (1:1000; LSL), a goat anti-mouse antibody against MMP9 (1:150; R&D), a mouse anti-mouse antibody against the aggrecan DIPEN neoepitope (1:100; ab3777; Abcam), and a rat anti-mouse antibody against CD34 clone MEC14.7 (1:50; Hycult Biotech) were used. For bromodeoxyuridine labeling, animals were injected intraperitoneally with bromodeoxyuridine (25 μg/g body weight; Sigma) 2 h prior to sacrifice, and the sections were stained with a bromodeoxyuridine staining kit (Zymed) according to the manufacturer's instructions.

*Viral Transfections and Osteoclastogenesis Assay*—For adenovirus infection of KLF5 to OUMS27 cells, the construction of adenovirus KLF5 expression vector was described previously (21). Adenovirus expressing KLF5 or the control empty vector (EV) was transduced to the cells at 40 or 100 multiplicities of infection. At 72 h after transfection, the cells were harvested and used for subsequent assays. For retrovirus infection of KLF5 to M-BMMΦ, the construction of retrovirus KLF5 expression vector was described previously (16). M-BMMΦ were infected with KLF5 or control retroviral particles and further cultured with M-CSF (30 ng/ml) and soluble RANKL (100 ng/ml) for 4–5 additional days, and then the number of cells positively stained for TRAP and containing more than three nuclei were counted as osteoclasts.

*RNA Interference*—Small interfering RNA oligonucleotides were constructed by DHARMACON. They were transfected to OUMS27 cells in concentrations of 200 nM, according to the manufacturer's instructions, and cultured for 72 h for subsequent assays. Small interfering RNA probe sequences are described in the supplemental materials.

*Real Time RT-PCR, Western Blotting, and Gelatin Zymography*—For RT-PCR, total RNAs were reverse-transcribed with MultiScribe reverse transcriptase (ABI). Real time PCR was performed on an ABI Prism 7000 sequence detection system (ABI) using QuantiTect SYBR Green PCR Master Mix (Qiagen), according to the manufacturer's instructions. Sequence information is described in the supplemental materials. For Western blot analysis, primary antibody to KLF5 (1:1000; KM1785) (15), MMP9 (1:1000; R&D), or β-actin (1:2000; Sigma) was used. For gelatin zymography, 10 μg of cell lysates was loaded to a zymogram acrylamide gel. The gel was electrophophoresed and incubated with developing buffer for 40 h using a Zymography Electrophoresis kit (Cell Garage).

*Microarray Analysis*—Target genes of KLF5 were identified by comparing mRNA expression in OUMS27 cells with adenoviral introduction of KLF5 or EV using two systems of microarray analyses: APHS-016 (for human extracellular matrix and adhesion molecules; supplemental Table 1) and APHS-024 (for human angiogenesis molecules; supplemental Table 2) in an RT2 Profiler PCR Array System (Super Array Bioscience). For MMP19 and -20 and ADAMTS4, -5, -9, and -15, which are not included in the array systems, real time RT-PCR analysis was separately performed. Sequence information is described in the supplemental materials.

*Luciferase Assay*—The human MMP9 promoter regions from −1,250 bp relative to the transcriptional start site were cloned into the pGL4-Basic vector (Promega). The luciferase assay was performed with a dual luciferase reporter assay system (Promega) using GloMax™ 96 Microplate Luminometer (Promega).

*Radiological Analyses*—Plain radiographs were taken using a soft x-ray apparatus (CMB-2, SOFTEX), and bone mineral density was measured by dual energy x-ray absorptiometry using a bone mineral analyzer (PIXImus, Lunar Corp.).

*Bone Fracture Experiment*—A transverse osteotomy was created at the midshaft of the right tibia using a bone saw and was internally stabilized with an intramedullary nail using the inner pin of a spinal needle of 22- or 23-gauge diameter depending on the size of the cavity, as we reported previously (22, 23). For histological analyses, specimens of the harvested tibias were fixed with 4% paraformaldehyde, decalcified with EDTA, dehydrated with ethanol, embedded in paraffin, and cut into 5-μm sections. The sections were stained with HE or toluidine blue.

*Arthritis Experiment*—Arthritis was induced by the modified method of Terato *et al.* (24, 25). Briefly, mice were injected intraperitoneally with 10 mg of an anti-COL2 monoclonal antibody (Immuno-Biological Laboratory) on day 0. On days 2 and 7, 50 μg of lipopolysaccharide (100 μl of 500 μg/ml solution in saline) was injected intraperitoneally, followed by an intermittent lipopolysaccharide injection every 3 days to the end of the experiment. As a control, 2.5 and 0.1 ml of saline was injected similarly to the antibody and lipopolysaccharide, respectively. The clinical severity of arthritis was graded on a 0–3 scale as follows: 0, normal; 1, swelling of ankle or wrist or limited to digits; 2, swelling of the entire paw; 3, maximal swelling. Each limb was graded by a single blinded observer, allowing a maximum arthritis score of 12 for each animal.

*Statistical Analysis*—Means of groups were compared by analysis of variance, and significance of differences was determined by *post hoc* testing using Bonferroni's method.

## RESULTS

*KLF5 Expression in Bone and Cartilage*—To know the involvement of KLF5 in skeletal metabolism, we initially examined the expression of KLF5 mRNA in cells of bone and cartilage by RT-PCR analysis (Fig. 1*A* and supplemental Fig. 1*A*). It was expressed in primary osteoblasts and chondrocytes derived from mouse neonatal calvaria and costal cartilage, respectively, as well as in osteoblastic cell line MC3T3E1 and chondrogenic cell lines ATDC5 and OUMS27. Meanwhile, the expression was hardly detected in osteoclasts formed from the precursor M-BMMΦ (20) or in monocyte-macrophagic cell line RAW264.7. Immunohistochemical analysis of tibial limbs of mouse embryos and neonates showed extensive expression of KLF5 in cells of all layers of cartilage and perichondrium as well as in osteoblasts on primary spongiosa (Fig. 1*B*). The expression in chondrocytes of limb cartilage was visible as early as E13.5 (supplemental Fig. 1*B*).

*Impaired Cartilage Degradation and Remodeling in KLF5$^{+/-}$ Limbs*—To learn the physiological function of KLF5 *in vivo*, we investigated the skeletal phenotype of KLF5$^{+/-}$ mice, because KLF5$^{-/-}$ mice died before E8.5 (15). Although KLF5$^{+/-}$ embryos (E16.5) showed normal skeletal patterning without abnormality in major organ development, they were smaller in size compared with wild-type littermates (Figs. 2, *A* and *B*). The femoral and tibial limbs of KLF5$^{+/-}$ embryos were 10–15% shorter than those of the wild-type littermates. In the KLF5$^{+/-}$ limb shaft, formation of bone and bone marrow tissues around

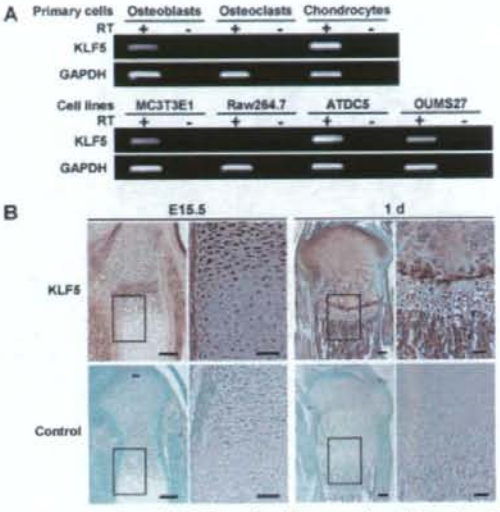


FIGURE 1. **Expression of KLF5 in cells of bone and cartilage.** *A*, mRNA expression of KLF5 and glyceraldehyde 3-phosphate dehydrogenase (*GAPDH*) as the loading control, determined by RT-PCR in mouse primary cells (*upper lanes*) (neonatal calvarial osteoblasts, mature osteoclasts formed from M-BMMΦ with M-CSF and RANKL stimulation, and neonatal costal chondrocytes) and cell lines (*lower lanes*) (osteoblastic cell line MC3T3E1, monocyte-macrophagic cell line Raw264.7, and chondrogenic cell lines ATDC5 and OUMS27). *B*, localization of KLF5 determined by immunohistochemistry by an antibody to KLF5 or the control nonimmune serum in tibial limbs of mouse embryo (E15.5) and neonate (1 day). The *inset boxes* in the *left panels* indicate the regions of the respective *right panels*. *Scale bars*, 100 and 50 μm in *left* and *right panels*, respectively.

the primary ossification center was delayed (Fig. 2*B*), and cartilage matrix like COL2 or COL10 remained undegraded in the shaft (Fig. 2*C*). Accordingly, TUNEL-positive apoptotic chondrocytes and tartrate-resistant acid phosphatase (TRAP)-positive osteoclasts/chondroclasts were decreased in the KLF5$^{+/-}$ limb. In the growth plate of neonates, although there was no difference in proliferative and prehypertrophic layers between the genotypes, the hypertrophic layer was elongated in KLF5$^{+/-}$ mice (Fig. 2, *D* and *E*). The Safranin-O-positive proteoglycan matrix remained in the hypertrophic layer, whereas the von Kossa-positive calcification layer was reduced in the KLF5$^{+/-}$ growth plate. These results indicate that the KLF5 insufficiency causes impairment of cartilage degradation and calcification in the perinatal period.

In an earlier period prior to the occurrence of ossification in the limb shaft of wild-type mice (E15.5), the limbs were filled with chondrocytes with comparable production of proteoglycan, COL10, and osteopontin in KLF5$^{+/-}$ and the wild-type littermates, indicating that KLF5 insufficiency did not affect chondrocyte differentiation in early stages up to hypertrophic differentiation (supplemental Fig. 2*A*). Chondrocyte proliferation determined by bromodeoxyuridine uptake was also similar between the genotypes (supplemental Fig. 2*B*).

After birth, skeletal growth of KLF5$^{+/-}$ mice caught up with that of wild type, and they became comparable at 4 weeks of age (supplemental Fig. 3, *A* and *B*). KLF5 did not affect bone remodeling after birth either, since bone density of KLF5$^{+/-}$ long bones was normal (supplemental Fig. 3, *C* and *D*).